

Computational approach to $(\text{ZnS})_i$ nanoclusters in ionic liquidsJon Zubeltzu ^{*}*Donostia International Physics Center (DIPC), 20018 Donostia, Euskadi, Spain;**Department of Applied Physics, Gipuzkoako Ingenieritza Eskola, Euskal Herriko Unibertsitatea (UPV/EHU),
20018 Donostia, Euskadi, Spain;**and Polymers and Advanced Materials: Physics, Chemistry and Technology Department, Kimika Fakultatea, Euskal Herriko Unibertsitatea
(UPV/EHU), 20018 Donostia, Euskadi, Spain*Jon M. Matxain  and Elixabete Rezabal *Donostia International Physics Center (DIPC), 20018 Donostia, Euskadi, Spain**and Polymers and Advanced Materials: Physics, Chemistry and Technology Department, Kimika Fakultatea,
Euskal Herriko Unibertsitatea (UPV/EHU), 20018 Donostia, Euskadi, Spain*

(Received 25 May 2021; accepted 20 July 2021; published 16 August 2021)

Unique and attractive properties have been predicted for II-VI-type semiconductor nanoclusters within the field of nanotechnology. However, the low reaction kinetics within the usual solvents gives only thermodynamic control during their production process, making the obtention of different metastable polymorphs extremely difficult. The use of ionic liquids as solvents has been proposed to overcome this problem. Identifying how these nanoclusters are solvated within ionic liquids is fundamental if this strategy is to be pursued. While computational chemistry tools are best suited for this task, the complexity and size of the system requires a careful design of the simulation protocol, which is put forward in this work. Taking as reference the $(\text{ZnS})_{12}$ nanocluster and the $[\text{EMIM}][\text{EtSO}_4]$ ionic liquid, we characterize the interactions between the nanoparticle and first solvation shell by density functional theory calculations, considering most of the solvent implicitly. The DFT results are consistent through different theory levels showing a strong interaction between the Zn atoms of the nanocluster and the $[\text{EtSO}_4^-]$ anion of the ionic liquid. A more realistic representation of the system is obtained by classical MD calculations, for which various classical force fields were considered and several atomic interactions parameterized. This new set of parameters correctly describes the interaction of different (ZnS) nanoclusters, supporting its transferability. The resulting MD simulation shows the formation of a structured ionic liquid solvation shell around the nanocluster with no exchange of ions for at least 5 ns, in agreement with the strong interactions observed in the density functional theory calculations.

DOI: [10.1103/PhysRevE.104.024604](https://doi.org/10.1103/PhysRevE.104.024604)**I. INTRODUCTION**

Nanoscience and nanotechnology have grown exponentially during the last decades, identifying a great number of new nanomaterials with novel and unique properties. In this aspect, II-VI semiconductors-based nanostructures have been deeply studied both experimentally and theoretically, and are promising materials for several technological and scientific purposes due to their unique optoelectronic properties: CdS and CdTe quantum dot based heterojunctions are expected to produce high efficiency photovoltaic devices, such as solar cells [1–9]. ZnO-, CdS-, and ZnS-based nanoclusters have shown unique catalytic features during photo and thermally driven chemical reactions [10–12]. ZnS-, CdS-, CdSe-, and ZnTe-based nanostructures are also promising for the fabrication of short-wavelength light emitting diodes and laser diodes [13]. This kind of nanostructures can be synthesised by several techniques: small 1–6 nm size nanostructures can be produced by top-down approaches, such as vapor deposition, although the size control of the products is less than the one achieved by

other experimental techniques [14]. Colloidal methods, however, have shown to produce monodisperse, size-controlled colloidal nanocrystals, usually 3–6 nm in size, and are nowadays well established for the whole group of II-VI materials [15]. However, due to their low reaction kinetics within the usual solvents, high temperatures are needed, giving only thermodynamic control of the production process and allowing to obtain the most stable polymorphs of the nanostructures [16–19]. Several studies based on computational simulations have predicted various metastable II-VI semiconductor-based nanocluster polymorphs, which nowadays cannot be experimentally synthesized in a controlled manner [20–33]. It has been predicted that with the proper control in the synthesis of the II-VI nanoclusters, properties could be tuned changing its size [20,23], new ones be added with the insertion of dopants [24–26,34], and more ambitiously, new crystals could be formed with different assemblings [27].

A novel proposed route to provide kinetic control over the production process of small II-VI nanoclusters at ambient temperatures is the use of ionic liquids (ILs) which could help in the kinetic control of the reaction to obtain nanoparticles of different polymorphs [35]. ILs are salts whose melting temperature is around or below ambient temperature and have

^{*}jon.zubeltzu@ehu.eus

attracted remarkable attention from chemists due to their great potential for diverse applications and the easy tunability of their physicochemical properties [36]. In particular, these nonconventional solvents have opened new perspectives for inorganic synthesis [37–41]. II-VI-type nanoparticles, being highly ionic materials, are expected to strongly interact with a highly polar media such as ILs, which has arose concerns about disintegration events on the nanoparticles. On the contrary, some ILs have proven to be useful as media for synthesizing ZnS [42–45], CdS [46,47], SnSe [48,49], and CdSe [50–53] nanostructures with the size of $2 \sim 3$ nm. One of the possible explanation for the stabilization of these kind of nanoclusters is the large viscosity of the ILs, 10 times higher than the usually employed conventional solvents (water and organic) [51]. Nevertheless, the strength and nature of such interactions and their impact on the nanocluster structure is yet to be determined [54].

ILs, consisting mainly of small anions with a rather localized charge and large cations with a disperse charge, are polyvalent materials due to their ability to establish interactions of different type with other molecules: from stable, directional, strong bonds, to weaker, fluctuating interactions. Therefore, one of the main tasks when addressing the influence of an IL environment in small nanocluster synthesis, is to establish the nature of their interaction. The works published in the literature so far do not reflect a clear interaction pattern for these types of clusters in IL, since contradictory and somewhat counterintuitive results have been obtained. Guleria *et al.* [51] claim that both ions of [EMIM][EtSO₄] contribute to the solvation of a CdSe nanoparticle; in particular, a strong bond is reported between Se and the O atom of the anion. On the other hand, Barzegar *et al.* [55] observe that CdS nanoparticles interact with the same IL via hydrogen bonds and electrostatic interactions between S atoms and the imidazolium cation.

Computational simulations are expected to be an ideal tool to tackle this, as they provide detailed information of the interactions from an atomistic and electronic point of view and avoid experimental costs. The fact that ILs establish long range interactions with the solutes requires big size systems to be considered, what is enabled by previously parameterized force-field-based classical simulations. At the same time, the specific, stable interactions that ILs may establish with the solutes are best described by quantum chemical calculations. However, the latter can only deal with relatively small systems. This is the main reason why only few studies can be found in the literature where different types of nanoparticles solvated by ILs are studied by means of quantum mechanical calculations [56–58]. Instead, this kind of systems have been more frequently studied in a larger scale by classical molecular dynamics (MD) calculations [59–68].

In this work, we establish a computational simulation protocol that combines quantum mechanical and classical molecular dynamics calculations to study the interaction of (ZnS)_i nanoclusters in imidazolium-based ILs efficiently. As IL solvent we choose the 1-ethyl-3-methyl imidazolium ethylsulfate ([EMIM][EtSO₄]), an imidazolium-based IL known to be an efficient solvent for ZnS [42,43], CdS [55], and CdSe [50,51] nanoparticles synthesis. As solute we choose the (ZnS)₁₂ nanocluster which has a diameter smaller than 2 nm [20], enabling a good compromise between system size and

computational cost. Obtaining a reliable description of such system will contribute to a better understanding on how (ZnS)_i nanoclusters, and more generally, II-VI-type nanoclusters behave towards this IL.

The choice of a particular theory level has to be adequated to the interactions of interest, due to the intrinsic limitations of each methodology. To the best of our knowledge, this is the first time that the system of choice is studied, and therefore, first of all, the nature of the interaction between the nanocluster and the IL has to be determined. Consequently, we start the theoretical approach at Density Functional Theory (DFT) level, which can describe reliably the interactions between the nanocluster and the IL pair of the first solvation shell. Due to the computational cost of the calculations, a small model will be chosen for this part. We will compare different exchange-correlation functionals, basis sets and hydrogen bond acidities of the implicit solvation model to check the consistency of the results throughout different theory levels and set the most adequate based on geometrical and energetic criteria.

Regarding the classical molecular dynamics calculations, several force fields are employed to represent the structure of the (ZnS)₁₂ nanocluster. We choose the most appropriate based on the results obtained by DFT calculations. Then, this force field is employed to perform classical MD calculations of the (ZnS)₁₂ nanocluster surrounded by the IL. To improve the description of the interactions between the IL and the (ZnS)₁₂ nanocluster, some of the inter-molecular interactions are parameterized to reproduce the results obtained by DFT. This will allow us to study large size systems that will adequately represent the influence of the bulk IL, while reproducing the DFT results on the nanocluster surface. The main objective of these simulations is to have a realistic idea of the solvation of nanoclusters in the IL, at an efficient theory level.

II. COMPUTATIONAL DETAILS

We carry out computational simulations at two theoretical levels: based on DFT and classical force fields. For the former, we carry out geometry optimizations and frequency calculations of the (ZnS)₁₂ nanocluster in the gas phase and solvated by the IL by the Gaussian16 package [69]. The IL is simulated by a cluster continuum approach, this is, with a explicit ionic pair of the solvent interacting directly with the cluster and the implicit representation of the rest of the solvent. Given the size of the model system, more accurate theory levels as post-Hartree Fock methods or triple- ζ quality basis sets are computationally too demanding. PBE has already been tested to be a reliable theory level in both ILs and nanoparticle studies separately, being widely used in the literature for such systems [54,70–73], and hence reference values will be obtained with this functional, taking into account dispersion interactions via Grimme's empirical dispersion term. Nevertheless, we ensure the consistency and stability of our results by assessing the influence of several exchange-correlation functionals: PBE-GD3BJ, B97D, wB97XD, and M11 (see Appendix A).

We choose as reference the SKBJ(10)-P/DZP basis set, as it has already shown to reliably describe the (ZnS)_i nanoclusters in the gas phase [21] and the IL, both independently [70,71]. In an attempt of defining a less demanding theory

level, we study the use of smaller basis sets: SKBJ(28)-P/SKBJ and SKBJ(28)-P/SKBJ-P. Further details can be found in Appendix A. To estimate the error introduced by the SKBJ(10)-P/DZP basis set, some of the free-energies are also calculated with the all electron 6-311++G(2df,2p) basis set. The solvation model based on density (SMD) [74] parameters are taken from a generic IL solvation model. We assess the influence of a generic and specific hydrogen bond acidity within this solvation model (see Appendix A).

To elucidate the nature of the interaction between the IL pairs and the nanocluster, both natural bond orbital [75,76] (NBO) and the quantum theory of atoms in molecules (QTAIM) [77,78] were used. Concretely, the interaction of the nanocluster with one IL pair was analyzed with both methods. NBO calculations were carried out using the PBE-GD3BJ functional, combined with the SKBJ(10)-P/DZP basis set. The implicit solvation model was included as described previously. Gaussian 16 program was used to perform such calculation. QTAIM calculations were performed with the same functional, combined with the 6-31G(d,p) all electron basis set for all atoms in this case, since core potentials may lead to misleading results. The AIMAll program [79] was applied to carry out such calculations.

For classical molecular dynamics calculations we use the LAMMPS code [80]. To choose a force field for the ZnS nanocluster, we optimize its structure employing three different polarizable force fields developed by Hamad *et al.* [81], Namsani *et al.* [82], and Wright *et al.* [83]. The three of them treat the S atoms by the core-shell model due to its larger polarizability compared to the Zn atoms. However, the force field by Wright *et al.* also considers the Zn atoms as polarizable particles. The basic form of the non-Coulombic interatomic potentials for the three of them takes the Buckingham potential form:

$$U_{ij}^{\text{short}} = A \exp\left(\frac{-r_{ij}}{\rho}\right) - Cr_{ij}^{-6}. \quad (1)$$

The detailed differences and similarities among these three force fields are discussed in Appendix B.

The intermolecular interactions between the (ZnS)₁₂ nanocluster and the IL ions are described by assigning Lennard-Jones parameters to all the different atomic species and applying the geometric combination rules in which the OPLS-AA framework is based. The parameters related with the Zn and S atoms of the nanocluster are the ones calculated by Namsani *et al.*, obtained to reproduce the DFT structure-energy of a Poly(methyl methacrylate)-(ZnS)₆ system [82]: $\epsilon_{\text{Zn}} = 0.954$ meV, $\sigma_{\text{Zn}} = 3.816$ Å, $\epsilon_{\text{S}} = 11.269$ meV and $\sigma_{\text{S}} = 4.270$ Å. However, the interaction between some of the atomic species are reparametrized into a Buckingham potential to correctly reproduce some of the results obtained by DFT calculations. This parametrization is carried out employing the GULP package [84,85], which minimizes the sum of square function. In our case, as it is later detailed in the text, we fit the Buckingham potential to reproduce the total energies of an interaction energy scan obtained by DFT.

The SHAKE algorithm [86] is applied to constrain the positions of the hydrogen atoms. At each timestep, the velocity-Verlet integrator is employed to predict the new positions and velocities of the particles. The long-range in-

teractions are computed by the particle-particle particle-mesh algorithm (PPPM) [87]. During the first 1 ns of the run, we adopt the NPT ensemble by applying the Nose-Hover barostat keeping the cubic shape of the simulation cell. Thereby, we obtain the equilibrated value of the volume at $P = 1$ atm and $T = 300$ K. Then the NVT ensemble is used by applying the Nose-Hover thermostat for 10 ns for the correct thermal equilibration of the system continued by 5 ns of production run. Previous works on pure ILs have shown that few ns of equilibration/production runs with hundreds of molecules are able to reproduce several experimentally obtained structural, energetic and dynamical properties of this kind of systems [88–90].

The polarizable particles are treated by the adiabatic core-shell model by Mitchell and Finchman [91] as coded in the “CORESHELL” package for LAMMPS [80]. This method is usually employed to model ionic/crystalline materials. To ensure robust and realistic trajectories and avoid possible issues caused by the use of the adiabatic core-shell model, the following is done: the relative motion of the core/shell pair is decoupled as an imaginary degree of freedom from the realistic system to maintain the internal kinetic energy of the core-shell pair. The velocity of the center of mass is computed and is rescaled for thermostating purposes. Possible momentum changes of the system caused by numerical fluctuations are avoided by setting the total momentum to zero. Given the large relative velocities of the shell and core particles with respect to their center of mass, we set a small timestep of 0.2 fs. It is important to notice that for the particular nanoclusters studied in this work a multiple-timestep integration scheme could be used to increase the efficiency of the simulations. However, one of the goals of this work is to set a consistent simulation method that enables the study of different size of (ZnS)_i nanoclusters or crystalline phases, for which high-frequency vibrations of the ions are expected [92], and therefore, the set of a small timestep is necessary for a correct description of these vibrations. In all the molecular dynamics simulations carried in this work the trajectories of the particles have remained stable.

III. RESULTS AND DISCUSSION

A. DFT

In this section we carry out DFT-based geometry optimizations and frequency calculations, evaluate the obtained results by different exchange-correlation functionals, basis sets, and bond acidities within the SMD method, and thereby establish the DFT part of the simulation protocol. The comparison is based on (i) the calculation of several energies and (ii) geometrical parameters.

Figure 1 shows the optimized structure of a (ZnS)₁₂ nanocluster and one pair of IL ions immersed in the implicit solvent obtained with the SKBJ(10)-P/DZP basis set and PBE-GD3BJ exchange-correlation functional. The structure obtained by the three different basis sets and four exchange-correlation functionals is qualitatively the same: a bond is formed between a positively charged Zn atom and a negatively charged O atom from the [EtSO₄⁻] anion, while the positively charged imidazol ring from the [EMIM⁺] cation tends to get

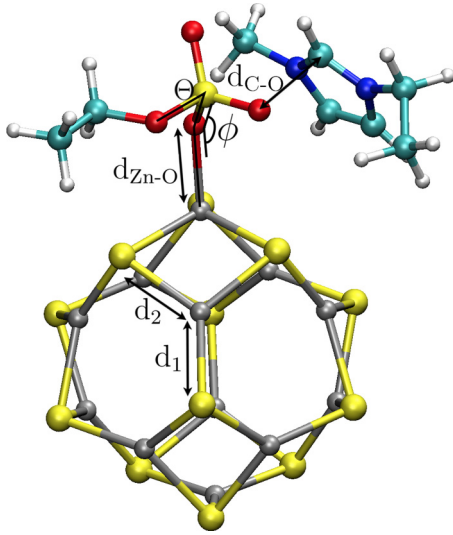


FIG. 1. Optimized structure of a $(\text{ZnS})_{12}$ nanocluster and one pair of IL ions immersed in the implicit solvent obtained with the SKBJ(10)-P/DZP basis set and PBE-GD3BJ exchange-correlation functional. The geometrical parameters d_1 , d_2 , $d_{\text{Zn-O}}$, $d_{\text{C-O}}$, ϕ , and Θ are used to evaluate the exchange-correlation functionals and basis sets.

close to another O atom of the $[\text{EtSO}_4^-]$ anion. The NBO method gives a charge of $-1.03e$ for the O atom that is bonded to the nanocluster. In the case of the implicitly solvated nanocluster we obtain the following charges of the Zn and S atoms from the nanocluster: $q_{\text{Zn}} = 0.91e$ and $q_{\text{S}} = -0.91e$. The opposite polarities observed for the O atom of the anion and Zn atoms of the nanocluster agrees with the attractive interactions and formation of bond observed between these atomic species as shown in Fig. 1. In the case of an implicitly solvated IL ion pair, the NBO method gives a net charge of $0.91e$ for the $[\text{EMIM}^+]$ cation and $-0.91e$ for the $[\text{EtSO}_4^-]$ anion. The decrease on the net charges of the ions agrees with previously reported results, where a charge transfer is observed due to the interaction between the ions of an IL [93].

1. Energetic and geometrical parameters

We calculate two different free energies: first, the interaction free energy (ΔG_1) between the $(\text{ZnS})_{12}$ nanocluster and one pair of IL, both in the gas phase, obtained by

$$\Delta G_1^{\text{gas}} = G_{\text{ZnS+IL}}^{\text{gas}} - (G_{\text{ZnS}}^{\text{gas}} + G_{\text{IL}}^{\text{gas}}), \quad (2)$$

where $G_{\text{ZnS}}^{\text{gas}}$, $G_{\text{IL}}^{\text{gas}}$, and $G_{\text{ZnS+IL}}^{\text{gas}}$ are the Gibbs free energies of an isolated $(\text{ZnS})_{12}$ nanocluster, an isolated pair of IL ions and a $(\text{ZnS})_{12}$ nanocluster with one pair of IL ions, respectively, all in their optimized geometries. Second, as an approximation of the solvation free energy, we calculate the implicit solvation free energy (ΔG_{S}) of a $(\text{ZnS})_{12}$ nanocluster with one pair of IL ions, obtained from

$$\Delta G_{\text{S}} = G_{\text{ZnS+IL}}^{\text{IL}} - G_{\text{ZnS+IL}}^{\text{gas}}, \quad (3)$$

where $G_{\text{ZnS+IL}}^{\text{gas}}$ and $G_{\text{ZnS+IL}}^{\text{IL}}$ are the Gibbs free energies of the $(\text{ZnS})_{12}$ nanocluster and one pair of IL ions in the gas phase and immersed in the implicit solvent, respectively. ΔG_{S} is calculated employing two different values of the hydrogen

bond acidity $\alpha_1 = 0.229$ and $\alpha_2 = 0.44$ within the SMD method, which we refer as ΔG_{S}^1 and ΔG_{S}^2 , respectively.

We measure six different geometrical parameters of the optimized structure of the $(\text{ZnS})_{12}$ nanocluster and one pair of IL ions, both in the gas phase and surrounded by the implicit IL solvent (see Fig. 1). The structure of the $(\text{ZnS})_{12}$ nanocluster is evaluated by the averaged values of d_1 and d_2 , both calculated without considering the bond lengths in which the Zn atom bonded to an O atom participates. Information about the interaction between the $(\text{ZnS})_{12}$ nanocluster and $[\text{EtSO}_4^-]$ anion is obtained by the bond length between the Zn and closest O_{S} atoms ($d_{\text{Zn-O}}$), angle formed by the Zn- O_{S} - S_{IL} atoms (ϕ) and dihedral angle formed by the Zn- O_{S} - S_{IL} - O_{C} atoms (Θ). We refer as O_{C} , S_{IL} and O_{S} to the O atom bonded with a C atom, S atom and O atom not bonded with a C atom, respectively, the three of them within the $[\text{EtSO}_4^-]$ anion. Given that the formation of strong bonds is observed between the $(\text{ZnS})_{12}$ nanocluster and $[\text{EtSO}_4^-]$ anions by DFT calculations, special attention is paid to accurately describe the latter geometrical parameters. The structural information related to the interaction between the $[\text{EMIM}^+]$ and $[\text{EtSO}_4^-]$ anions is obtained from the distance between the C_{N} atom and the closest O_{S} atom of the $[\text{EtSO}_4^-]$ anion ($d_{\text{C-O}}$). We refer as C_{N} to the C atom bonded to two N atoms of the imidazole ring.

All the energetic and geometrical parameters obtained with the different basis sets, exchange-correlation functionals and hydrogen bond acidities considered in this work are reported Appendixes C and D. The energy differences that are obtained with $\alpha_1 = 0.229$ and $\alpha_2 = 0.44$ employing the SKBJ(10)-P/DZP basis set are smaller than 2.0 kcal/mol. These differences are small enough to consider that the results are not significantly altered when using the specific hydrogen bond acidity instead of the most general one, and therefore, in the following only the more general value of the hydrogen bond acidity $\alpha = 0.229$ will be considered.

The comparison between the solvation and interaction free energies obtained by the SKBJ(28)-P/SKBJ-P and SKBJ(10)-P/DZP basis sets (see Appendix C) show substantial differences for all DFs chosen; for example, the wB97XD functional lowers the interaction energy by around 6 kcal/mol. The solvation energies decrease around 20-25 kcal/mol in the case of PBE-GD3BJ, B97D, and wB97XD. The analysis of the geometrical parameters also shows considerable changes when the basis set is decreased independently of the employed exchange-correlation functional: the distance $d_{\text{Zn-O}}$ changes at least 0.06 Å in all cases. Moreover, the four different functionals show a large difference in at least another geometrical parameter in the solvated system: for the PBE-GD3BJ and wB97XD functionals the averaged bond distance $\langle d_2 \rangle$ decreases more than 0.03 Å. In the case of the M11 and B97D functionals, $d_{\text{C-O}}$ shows a difference of -0.027 Å and 0.068 Å, respectively. Therefore, considering that the SKBJ(10)-P/DZP basis set have been previously assessed and used in the literature, we conclude that albeit the SKBJ(28)-P-based basis set implies less computational effort, it does not provide a satisfactory representation of the system.

Table I shows the values of the interaction and implicit solvation free energies obtained with the SKBJ(10)-P/DZP basis set, $\alpha = 0.229$ hydrogen bond acidity and different

TABLE I. Interaction ($\Delta G_{\text{I}}^{\text{gas}}$) and implicit solvation ($\Delta G_{\text{S}}^{\text{l}}$) free energies of a (ZnS)₁₂ nanocluster and one pair of IL ions obtained with four exchange-correlation functionals.

E_{xc}	$\Delta G_{\text{I}}^{\text{gas}}$ (kcal/mol)	$\Delta G_{\text{S}}^{\text{l}}$ (kcal/mol)
PBE-GD3BJ	-25.5	-74.5
M11	-25.5	-102.2
B97D	-22.5	-84.5
wB97XD	-24.3	-88.4

exchange-correlation functionals considered in this work. When compared to the result obtained with the PBE-GD3BJ functional, we observe similar interaction free energies $\Delta G_{\text{I}}^{\text{gas}}$ (up to a difference of 3 kcal/mol for the case of the wB97XD functional). The solvation free energies $\Delta G_{\text{S}}^{\text{l}}$, however, show larger differences: B97D and wB97XD differ by 10-14 kcal/mol, while the M11 functional gives a large deviation of 27.8 kcal/mol. The latter can be related with a non expected effect observed on the geometrical parameter $d_{\text{C-O}}$: when the gaseous system is solvated employing the M11 functional, its value decreases from 2.943 Å to 2.941 Å. The bond distances are expected to increase when a gaseous system is solvated as a consequence of the interaction with the solvent [94], as occurs with all the chosen functionals except for this particular one. We observe that all functionals show similar geometrical parameters. All the distance deviations are not larger than 0.04 Å with respect to the ones obtained with the PBE-GD3BJ functional, while the maximum angular deviation is 4°. The detailed discussion on the obtained geometrical parameters is reported as Appendix D.

We further analyze the consistency of the PBE-GD3BJ functional and quantitatively evaluate the error introduced by the SKBJ(10)-P/DZP basis set by calculating several free energies describing all the atoms of the system by a 6-311G**(2d,2f) basis set. Given that the calculations with such a large basis set imply large computational cost, we only calculate the interaction free energy $\Delta G_{\text{I}}^{\text{gas}}$ of the system in the gas phase in two configurations: on the one hand, maintaining the positions of the atoms obtained from the optimization calculations with the SKBJ(10)-P/DZP basis set and, on the other hand, with the optimized structure calculated with the 6-311G**(2d,2f) basis set. The latter has been carried out only with the PBE-GD3BJ and B97D functionals, given that these are computationally expensive calculations, and among the different functionals, the B97D functional is the one giving the largest structural deviations from the PBE-GD3BJ functional (described in detail in Appendix D). Finally, the difference between these free energies with the ones obtained with the SKBJ(10)-P/DZP basis set are calculated. For the sake of clarity, we referred to the former and the latter as $\Delta G_{\text{I}}^{\text{gas-1}}$ and $\Delta G_{\text{I}}^{\text{gas-2}}$, respectively. Table II shows the differences in interaction free energies for each density functional and type of structure.

For a given functional the interaction free energy differences are similar for both types of structures, indicating small changes between the optimized structures obtained with the 6-311G**(2d,2f) and SKBJ(10)-P/DZP basis sets. The

TABLE II. Interaction free energy differences obtained with the SKBJ(10)-P/DZP and 6-311G**(2d,2f) basis sets for each type of structure (see text) and four exchange-correlation functionals.

Structure	E_{xc}	$\Delta G_{\text{I}}^{\text{gas-2}} - \Delta G_{\text{I}}^{\text{gas-1}}$ (kcal/mol)
SKBJ(10)-P/DZP	PBE-GD3BJ	5.3
	B97D	4.8
	M11	5.0
	wB97XD	3.4
311G**(2d,2f)	PBE-GD3BJ	5.1
	B97D	4.4

SKBJ(10)-P/DZP basis set introduces an overestimation of about 4–5 kcal/mol in the interaction free energy. However, given that the energy scan calculations (see later in the text) estimate an interaction energy of about 30 kcal/mol, we conclude that the description of the system with the SKBJ(10)-P/DZP basis set properly captures the nature of the interactions between the IL and the nanocluster. Moreover, the use of the 6-311G**(2d,2f) basis set would substantially increase the computational effort of the DFT-based part of the theoretical protocol, and considerably limit the computation capability to study systems made of larger nanoclusters solvated in ILs. Thereby, having estimated the error that is introduced in the following calculations by the SKBJ(10)-P/DZP basis set, we adopt this particular basis set for the DFT part of the theoretical protocol. Regarding the influence of the particular functional chosen, Table II shows a consistent increase of about 4–5 kcal/mol independently of the employed functional, that together with the geometrical results obtained previously, suggest that no undesired artifact is introduced by the choice of the PBE-GD3BJ functional. Thereby, the PBE-GD3BJ functional is chosen as the functional to be employed in the DFT-based part of the simulation protocol.

2. Zn-O_s interaction analysis

Once the DFT protocol has been established, the analysis of the interaction between one IL pair and the nanocluster has been performed on the optimized structure, by means of the atomic charges, NBO and QTAIM methods. As already described above (see Fig. 1), the main interaction is the one occurring between one of the oxygen atoms of the anion and one of the zinc atoms of the cluster. Before moving on to deeper analysis, we first focus on the charges obtained by the NBO method. According to these values (−1.03e for the O and 0.87e for the Zn atom) the electrostatic nature of the interaction should be large. The NBO and QTAIM analysis provide more light on this.

According to the NBO analysis, there is no natural bond orbital between these two atoms. Instead, there is a Zn-oriented lone-pair on O atom with occupation 1.914, and an empty Zn orbital with occupation 0.180. The second order interaction between these two orbitals is around 30 kcal/mol. Hence, NBO agrees with the electrostatic interaction, and shows a donor-acceptor character where the oxygen lone-pair is oriented towards the zinc atom.

QTAIM analysis focuses on the electron density analysis. Calculated values at the Zn-O bond critical point are

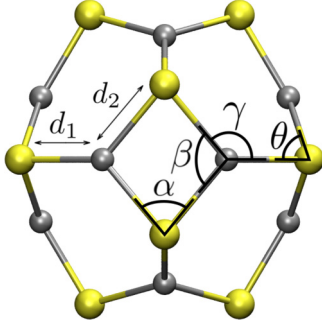


FIG. 2. Structure of the $(\text{ZnS})_{12}$ nanocluster made of six rhombic and eight hexagonal atomic rings. The Zn and S atoms are represented in gray and yellow, respectively. The formed bond lengths d_1 and d_2 and angles α , β , γ , and θ are the geometrical parameters employed for comparison of the force fields (see Table I).

the following: $\rho = 0.0659$ a.u., $\nabla^2\rho = 0.3059$ a.u., $V = -0.0967$ a.u., and $G = 0.0866$ a.u. For a covalent interaction, the following conditions should be fulfilled: $|V| \geq 2G$ and $\nabla^2\rho < 0$. Clearly, this is not the case, and hence we conclude that the interaction is not covalent, but electrostatic. However, the large value of ρ (about three times larger than in H bonding [95,96]) and the negative value of $H = G + V$ suggest that the interaction should be considered as partially covalent in nature.

Taking all these analyses into account, we may conclude that the interaction between the IL and the nanocluster is mostly electrostatic, with a partial covalent bond coming from the donor-acceptor interaction between the lone pair of the O atom and the empty orbital of the Zn atom. This type of interaction is compatible with the calculated interaction energy of 25.5 kcal/mol, given in Table I for PBE-GD3BJ combined with the SKBJ(10)-P/DZP.

B. Force field

First of all, an adequate force field for representing the nanocluster will be established. Figure 2 shows the optimized structure of a $(\text{ZnS})_{12}$ nanocluster in the gas phase by DFT calculations with the PBE-GD3BJ exchange-correlation functional and the SKBJ(10)-P/DZP basis set. We observe two characteristic Zn-S bond lengths (d_1 and d_2), Zn-S-Zn angles (α and θ), and S-Zn-S angles (β and γ) repeated throughout the nanocluster. We optimize the structure of the nanocluster in the gas phase with each force-field and compare these geometrical parameters by calculating the absolute deviation

of each bond length:

$$\Delta d = d - d^{\text{DFT}}, \quad (4)$$

where d^{DFT} is the bond length obtained by DFT calculations, and the percentage of the relative angular deviation:

$$\Delta\alpha = \frac{100(\alpha - \alpha^{\text{DFT}})}{\alpha^{\text{DFT}}}, \quad (5)$$

where α^{DFT} is the characteristic angle obtained by DFT calculations.

The obtained bond lengths, angles, and respective deviations are shown in Table III. A reasonably small angular deviation is given by the Hamad *et al.* model, giving the smallest deviation of the β angle among the three models. However, the bond deviations are considerably large: $\Delta d_1 = 0.39$ Å and $\Delta d_2 = 0.41$ Å. Although the force-field by Wright *et al.* gives the smallest deviations of the bond lengths $\Delta d_1 = -0.01$ Å and $\Delta d_2 = -0.04$ Å, it also shows the largest angular deviations for all the angles, indicating that the shape of the nanocluster deviates with respect to the referential one. The force-field by Namsani *et al.* shows a reasonably good agreement with respect to the bond lengths, giving deviations larger than the ones by Wright *et al.* but within the same order of magnitude. Moreover, out of the four characteristic angles, three (α , γ , and θ) give the smallest angular deviations. Therefore, we conclude that the force-field developed by Namsani *et al.* [82] gives the best balance between the description of the bond distances and angles within the nanocluster in general. In addition to these results, this same force-field [82] has already shown to reproduce with high accuracy several experimental structural and elastic properties of ZnS bulk on its wurtzite and zincblende phases, such as elastic constants, bulk moduli and static and high-frequency dielectric constants. Taking into account the previous observations, we decide to choose the force-field by Namsani *et al.* for the molecular dynamics calculations.

C. Parametrization of the nanocluster-IL interaction

For the classical MD calculations we assign the Lennard-Jones parameters given by Namsani *et al.* [82] to the Zn and S atoms of the nanocluster to describe the intermolecular interactions between the atoms from the nanocluster and the IL ions. However, these parameters were calculated by taking into account the interactions between neutral molecules. Our system differs strongly from this picture: half of the ions that compose the IL are positively charged, while the other half are negatively charged. Moreover, the DFT calculations show a strong interaction between the negatively charged EtSO_4^-

TABLE III. Geometrical parameters (see Fig. 2) and deviations for a $(\text{ZnS})_{12}$ nanocluster obtained by DFT calculations and three different force-fields. The values of the parameters closest to the ones obtained by DFT are marked by an asterisk (*).

DFT	d_1 (Å)	Δd_1 (Å)	d_2 (Å)	Δd_2 (Å)	α	$\Delta\alpha$	β	$\Delta\beta$	γ	$\Delta\gamma$	θ	$\Delta\theta$
Namsani <i>et al.</i>	2.29	-0.06	2.17	-0.10	84.13*	8.95	93.78	-3.97	127.04*	-2.34	110.84*	8.98
Hamad <i>et al.</i>	2.74	0.39	2.68	0.41	84.73	9.73	95.41*	-2.30	123.79	-4.84	115.08	13.15
Wright <i>et al.</i>	2.34*	-0.01	2.23*	-0.04	89.13	15.42	90.86	-6.96	119.26	-8.32	120.78	18.75

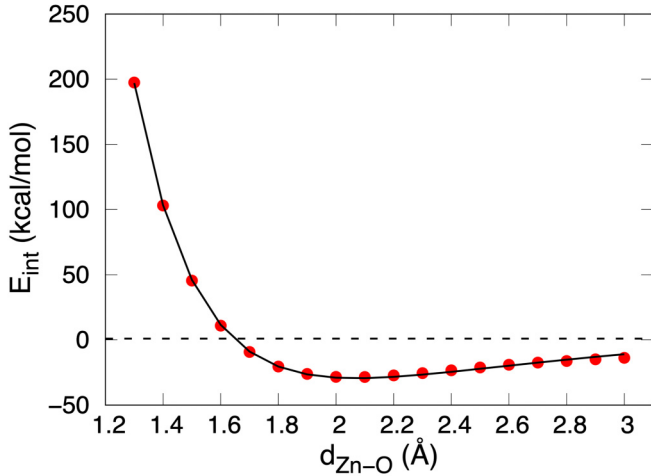


FIG. 3. Interaction energy of a (ZnS)₁₂ nanocluster with one pair of IL ions implicitly solvated as a function of the Zn-O_S distance (see Fig. 1) obtained with DFT (red points) and fitted reparametrized classical force field (black line).

anion and the nanocluster. Considering these observations, we decide to parametrize the potential interaction between the Zn and S atoms of the nanocluster with the O_S atoms of the EtSO₄ anion to ensure an optimal description of their interactions.

We calculate the scan of the interaction energy between the nanocluster and the EtSO₄ anion. Ideally, one could obtain a more reliable interaction energy by including explicitly the rest of the ions of the IL and placing them at different positions for each energy scan. However, this would increase substantially the complexity of the calculation, and therefore, we assume that the largest part of the interaction relies on the S-O_S bond and the influence of the bulk is in part captured by the implicit solvent model. The scan is carried out as follows: we freeze the position of the atoms in Fig. 1, where most of the IL is represented by the implicit solvation model, and scan the interaction energy of the system moving the IL ions along the bond direction of the Zn atom of the nanocluster and closest O_S atom of the IL by DFT calculations with the PBE-GD3BJ exchange-correlation functional and the SKBJ(10)-P/DZP basis set. Then, these observables are used to fit the parameters of the interaction potentials between the Zn-O_S and S-O_S pairs of atomic species. These interaction potentials take the form of a Buckingham potential. The red points in Fig. 3 show the interaction energy of the system for several values of $d_{\text{Zn-O}}$ calculated by DFT, while the black line is obtained with the fitted Buckingham potential parameters (see Table IV). As shown in the Fig. 3, the agreement between the interaction energies calculated with both methods is large and satisfactory.

TABLE IV. Fitted Buckingham potential parameters [see Eq. (B1)] for the Zn-O and S-O interactions.

Interaction	A (kcal/mol)	ρ (Å)	C (Å ⁶ kcal/mol)
Zn-O	26154.48	0.25	$8.85 \cdot 10^{-5}$
S-O	3475.14	0.23	–

To check the transferability of the obtained potential parameters, we now analyze the interaction energy of the IL with other ZnS nanocluster polymorphs. Given that the (ZnS)₁₂ nanocluster belongs to the hollow bubblelike structural family, we chose two nanoclusters that differ either on the structure or the number of atoms that is composed of. For the former, we chose the (ZnS)₁₃ [20,22] metastable polymorph as it has a similar number of atoms but shows a wurtzitelike structure. For the latter, the (ZnS)₂₄ nanocluster is employed due to its similar hollow bubblelike structure and larger number of atoms [20]. The interaction energy scans obtained by DFT and classical force field are shown in Fig. 4. In the case of the (ZnS)₁₃ nanocluster, the interaction energies given by the DFT and classical force-field calculations are $E^{\text{DFT}}(2.1 \text{ \AA}) = -29.1 \text{ kcal/mol}$ and $E^{\text{CFE}}(2.0 \text{ \AA}) = -31.6 \text{ kcal/mol}$, respectively, while in the case of the (ZnS)₂₄ nanocluster we obtain $E^{\text{DFT}}(2.1 \text{ \AA}) = -29.9 \text{ kcal/mol}$ and $E^{\text{CFE}}(2.0 \text{ \AA}) = -30.2 \text{ kcal/mol}$. Taking into account that the global picture of both scans and the position and value of the interaction energies obtained largely agree, we obtain solid indications for the reliable use of the reparametrized classical force field to study different polymorphs of ZnS nanoclusters solvated by the [EMIM][EtSO₄] IL. In addition to that, the strong agreement shown by the two calculation methods in both systems indicates that, the parametrization of only the interaction between the Zn-O and S-O interatomic species captures the interaction between the different ions of the system. Thereby, we include these new parameters in the previous force field and study the solvation of the nanocluster by means of classical molecular dynamics.

D. Molecular Dynamics: Random initial configuration

We first fix the position of the (ZnS)₁₂ nanocluster in the center of the simulation box with dimensions $(55 \times 55 \times 55) \text{ \AA}^3$ and fill the rest of the box with 300 pairs of IL ions randomly positioned. Then, an NPT run is carried out at $T = 300 \text{ K}$ and $P = 1 \text{ atm}$. Figure 5 shows the time evolution of the pressure and density of the system. Their respective cumulative running averages stay almost constant after the first 400 ps of the run, indicating a small uncertainty in our averaged density value. Averaging the volume of the system during the last 100 ps of the annealing, we obtain an equilibrated simulation box of dimensions $(45.938 \times 45.938 \times 45.938) \text{ \AA}^3$, which gives a density of $\rho = 1.234 \text{ g cm}^{-3}$.

Then, we fix the NVT ensemble for a 10 ns annealing run ensuring a correct thermal equilibration of the system followed by 5 ns of production run. The structural analysis is carried out by calculating the radial distribution function $g(r)$ and its integral over a sphere of radius r , or simply called coordination number function $N(r)$.

In the top panels of Fig. 6 the $g(r)$ between the center of mass of the (ZnS)₁₂ nanocluster (CM) and different atomic species is shown: S and Zn atoms from the (ZnS)₁₂ nanocluster, O_S and S_{IL} atoms from the [EtSO₄⁻] anions, and center of mass (CM_N), N and H_N atoms of the [EMIM⁺] anion. The lower panels show the respective $N(r)$ functions except for the CM-Zn and CM-S pairs. For the sake of clarity, these two functions have not been included in the figure as it is straightforward to determine their value at large distances

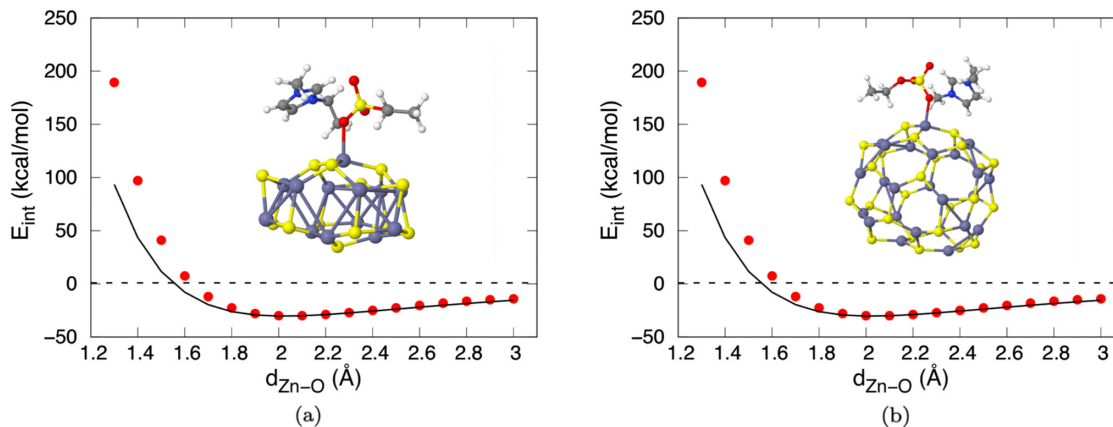


FIG. 4. Interaction energy of a (a) $(\text{ZnS})_{13}$ and (b) $(\text{ZnS})_{24}$ nanocluster with one pair of IL ions implicitly solvated as a function of the Zn-O_S distance obtained with DFT (red points) and reparametrized classical force-field (black line).

($N_{\text{CM-S}}(r) = N_{\text{CM-Zn}}(r) = 12$). We refer as H_N to the most acidic H atom from [EMIM⁺] cations, the one that is bonded to the C_N atom.

For comparison, we also show the radial distribution function $g_h(r) = 1$ and coordination number function N_h of an ideally uncorrelated liquid. The latter is obtained by

$$N_h(r) = \frac{4\pi r^3 n}{3V}, \quad (6)$$

where n is the total number of particles of a given species within a simulation box with volume V . The upper panel in Fig. 6 shows N_h considering the number of O_S ($n = 900$), N ($n = 600$), and S_{IL}, CM_N, and H_N ($n = 300$) atoms in our simulation box.

Looking at $g_{\text{CM-Zn}}(r)$ and $g_{\text{CM-S}}(r)$ in Fig. 6 we observe that the Zn atoms are closer to the CM than the S atoms, similarly to what occurs when the nanocluster is in the gas phase (see Fig. 2) and also in implicit solvent. Their maxima show large values: $g_{\text{CM-Zn}}(3.45 \text{ \AA}) = 2259$ and $g_{\text{CM-S}}(3.65 \text{ \AA}) = 1962$. This is due to the low density of these atomic species in the simulation box.

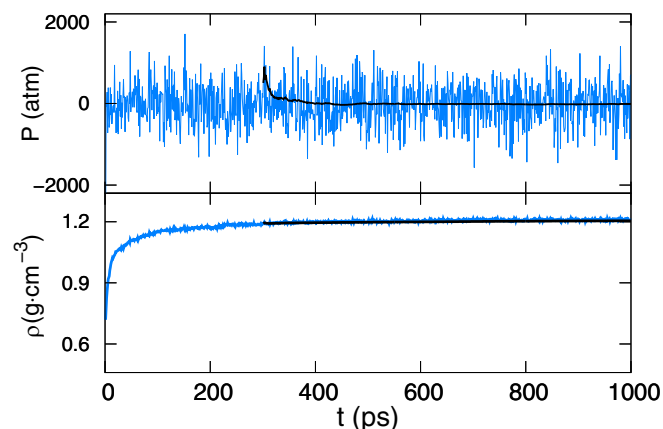


FIG. 5. Evolution of the pressure (upper panel) and density (lower panel) of the system during 1 ns of the NPT run. The blue line shows the instantaneous values, while the black line shows the cumulative running average starting from $t = 300$ ps.

From the comparison between Figs. 6(a) and 6(b) we conclude that the [EtSO₄⁻] anions are more structured around the nanocluster than the [EMIM⁺] cations: $g_{\text{CM-S}_{\text{IL}}}(r)$ and $g_{\text{CM-O}_S}(r)$ show larger and narrower first neighbor peaks than $g_{\text{CM-N}}(r)$, $g_{\text{CM-H}_N}(r)$ and $g_{\text{CM-CM}_N}(r)$. However, it is important to note that still these radial distribution functions show clear first neighbor peaks that decay almost to zero in their first minimum: $g_{\text{CM-N}}(10.05 \text{ \AA}) = 0.108$, $g_{\text{CM-H}_N}(8.25 \text{ \AA}) = 0.022$ and $g_{\text{CM-CM}_N}(10.35 \text{ \AA}) = 0.024$. These low values indicate the appearance of a structured first solvation shell around the nanocluster of [EMIM⁺] cations.

This structuring effect is larger in the case of the [EtSO₄⁻] anions. After the pronounced first-neighbor peaks that show $g_{\text{CM-S}_{\text{IL}}}(r)$ and $g_{\text{CM-O}_S}(r)$ in Fig. 6(a), both functions decay to zero. This means that during the 5 ns of the production run there has not been any exchange of [EtSO₄⁻] anions between the first solvation shell and the rest of the liquid. The upper panel in Fig. 6 supports the previous observation: $N_{\text{CM-O}_S}(r)$ shows two strong plateaus at $N = 9$ and 27, while $N_{\text{CM-S}_{\text{IL}}}(r)$ shows one at $N = 9$, indicating the presence of nine strongly bonded sulfates from nine [EtSO₄⁻] anions during 5 ns. These sulfates are expected to be bonded to certain Zn atoms of the nanocluster, as observed in the DFT calculations for the small model. We check this by analyzing the radial distribution function and coordination number function between the Zn atoms of the nanocluster and the O_S and S_{IL} atoms of the [EtSO₄⁻] anions. This is shown in Fig. 7.

Both radial distribution functions show a pronounced first neighbor peak: $g_{\text{Zn-S}_{\text{IL}}}(3.36 \text{ \AA}) = 8.59$ and $g_{\text{Zn-O}_S}(1.92 \text{ \AA}) = 7.97$. Note that the first neighbor peak of $g_{\text{Zn-S}_{\text{IL}}}$ is located 1.44 Å away from the one of $g_{\text{Zn-O}_S}$. Taking into account that the bond distance between the O_S and S_{IL} atoms of the [EtSO₄⁻] anion is 1.42 Å, we deduce that these inter-coordinated Zn, O_S and S_{IL} atoms are located close to a straight line. Between the first and second neighbor peaks both RDFs decay to zero in agreement with the previous analysis. This supports the appearance of a structured first solvation shell of IL ions around the nanocluster.

The $N_{\text{Zn-S}_{\text{IL}}}$ and $N_{\text{Zn-O}_S}$ functions in Fig. 7 show a plateau at $N = 9/12 = 0.75$, indicating that out of the 12 Zn atoms that conform the $(\text{ZnS})_{12}$ nanocluster, nine are in average

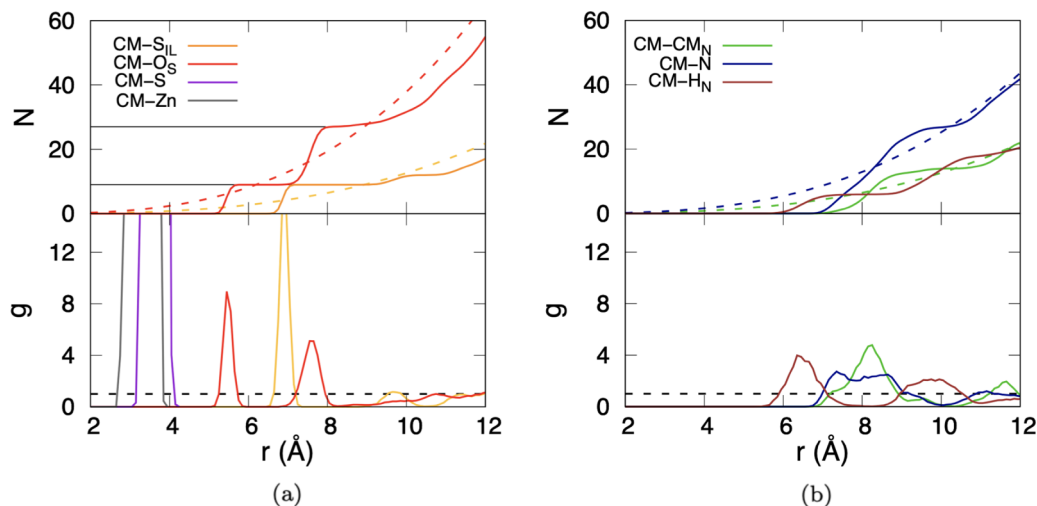


FIG. 6. Coordination number functions (upper panels) and radial distribution functions (lower panels) between the center of mass of the $(ZnS)_{12}$ nanocluster and several atomic species: (a) Zn (gray) and S (purple) atoms of the nanocluster, O_S (red) and S_{IL} (orange) atoms from the $[EtSO_4^-]$ anions, and (b) center of mass (green), N (blue) and H_N (brown) particles of the $[EMIM^+]$ cations. The colored dashed lines in the upper panels show $N_h(r)$ (see text) calculated for the CM_N and H_N (green), N (blue), O_S (red) and S (orange) atoms. (a) The horizontal lines at $N = 9$ and $N = 27$ indicate plateaus in $N_{CM-O}(r)$ and $N_{CM-S_{IL}}(r)$.

strongly coordinated to those O_S atoms. Moreover, we observe that during the 5 ns of the production run each of the nine Zn atoms have been coordinated with one single and same O_S atom, while the remaining three Zn atoms have not been coordinated with any O_S atom. These results indicate that a structured solvation shell of nine $[EtSO_4^-]$ anions is formed around the nanocluster that lasts for at least 5 ns. Supposing that an uncoordination event occurs between one pair of Zn- O_S atoms right after the 5 ns of production run and considering that these uncoordination events are independent among them,

we obtain that the Zn- O_S coordination lifetime is at least of 22.5 ns. Notice that this long time is in agreement with the calculated interaction energies and with the nature of the Zn-O chemical bond. The reason why only nine out of 12 Zn atoms are coordinated (the nanocluster could be fully coordinated) by only one O atom (they could be doubly coordinated) still remains unclear, and a possible study as future perspective could be to check whether this partial solvation pattern is maintained for different nanocluster types and sizes.

We analyze the spacial distribution of the nine coordinated $[EtSO_4^-]$ anions with the nine Zn atoms. Figure 8(a) shows a snapshot of the distribution of the nine coordinated O_S atoms from the $[EtSO_4^-]$ anions around the nanocluster. It is convenient for the analysis to note that each Zn atom from the nanocluster has one first neighbor Zn atom. The 12 Zn atoms of the nanocluster can be classified into six pairs of first neighbor Zn-Zn atoms that belong to a Zn-S-Zn-S rhombic atomic ring [see Fig. 8(b)]. These six rhombic atomic rings are distributed equidistantly within the nanocluster.

These O_S atoms are homogeneously distributed around the nanocluster: given that nine O_S atoms are coordinated with the nanocluster, and each of those tends to coordinate with

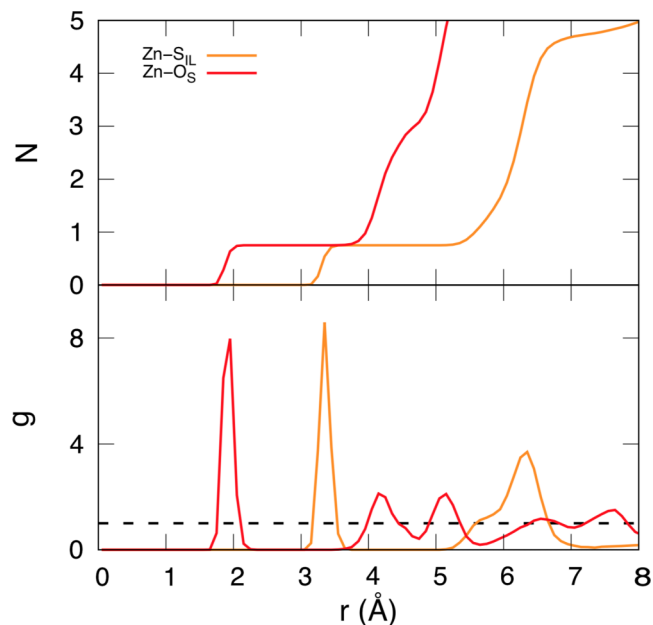


FIG. 7. Coordination number functions (upper panel) and radial distribution functions (lower panel) between the Zn atom of the nanocluster and different atomic species: O_S (red) and S_{IL} (orange) atoms from the $[EtSO_4^-]$ anions.

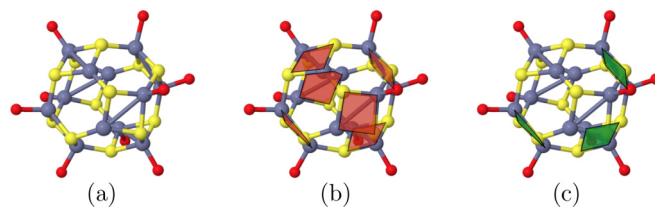


FIG. 8. (a) Snapshot of the distribution of the nine coordinated O_S atoms from the the $[EtSO_4^-]$ anions around the nanocluster. Highlight of (b) the six Zn-S-Zn-S rhombic atomic rings (red rhombuses) that make up the $(Zn-S)_{12}$ nanocluster and (c) the three Zn-S-Zn-S rhombic atomic rings doubly coordinated with O_S atoms (green rhombuses).

a single Zn atom, six out of the nine O_S atoms coordinate with the six rhombic atomic rings. In other words, all the six rhombic atomic rings are at least coordinated with one O_S atom [see Fig. 8(b)]. The remaining three O_S are coordinated with other three rhombic atomic rings that are coordinated with another O_S atom at the same time. These three doubly coordinated rhombic atomic rings are highlighted in Fig. 8(c). Note that the three doubly coordinated rhombic atomic rings chosen by the system are in the configuration (among others) in which the three doubly coordinated rhombic atomic rings are further away from each other. We conclude that given the nine intermolecular coordinations observed in the system, the $[EtSO_4^-]$ anions are spatially distributed in the most homogeneous way.

These results significantly differ from several previous experimental works: Guleria *et al.* [51] synthesized CdSe nanoparticles (II-VI semiconductor family) solvated with the same IL studied in our work. They conclude that while both ions interact with the nanoparticle, the prevailing interaction is the one between the imidazolium cation and the CdSe nanoparticle. Moreover, the formation of Se-O bonds between the nanoparticle and the anion of the IL is claimed. Another experimental work by Barzegar *et al.* [55] claim that the interaction between a CdS nanoparticle and the same IL occurs through S-cation interactions. These observations strongly differ with our simulations, where we observe significant interactions between the positively charged ion of the nanocluster and the O atom of the anion.

E. Molecular Dynamics: Fully coordinated initial configuration

To verify whether the obtained results are reliable and do not depend on the initial random configuration we start the simulation with, we carry out the same MD simulations from a different initial configuration: 12 $[EtSO_4^-]$ anions are placed to be coordinated with the 12 Zn atoms from the nanocluster. To do so, we take into account the first neighbor peak positions of $g_{Zn-S_{IL}}$ and g_{Zn-O_S} , located at $r = 3.36 \text{ \AA}$ and 1.92 \AA , respectively (see Fig. 7). We place 12 $[EtSO_4^-]$ anions so that the S_{IL} atom and one of the O_S atoms from each anion sit at these mentioned distances from each Zn atoms. In the following step, we add another 12 $[EMIM^+]$ cation randomly placed around the $(ZnS)_{12}$ nanocluster. Finally, this configuration of the nanocluster with 12 IL ions is placed in the center of the simulation box and it is filled with another randomly placed 288 IL ions. The rest of the simulation setup is the one employed in the previous MD simulations. In the following analysis, this initial configuration is referred to as the fully coordinated initial configuration.

Figure 9 shows the RDFs and coordination number functions between the center of mass of the $(ZnS)_{12}$ nanocluster and several atomic species of the IL ions obtained from the fully coordinated and random initial configurations. Despite slight differences, the agreement between all the shown functions is large: the value and position of the neighbor-peaks are very similar, while the coordination number functions are almost identical. In the case of the $N_{Zn-S_{IL}}$ and N_{Zn-O_S} functions obtained from the fully coordinated initial configuration, both show a plateau at $N = 9$ as in Fig. 6(a). We obtain the same final state as in the case of the random initial configuration:

during the 5 ns of the production run nine Zn atoms have been coordinated with other nine O_S atoms, while the remaining three Zn atoms have not been coordinated to any other O_S atom. Note that the fully coordinated (12 O_S atoms coordinated) and random (no O_S coordinated) configurations end up showing the same final state, where nine O_S are coordinated with nine Zn atoms from the nanocluster. This strongly indicates that in both cases stability has been reached by the system and supports the reliability of the obtained results.

IV. CONCLUSIONS

In this work we present a simulation protocol based on DFT and classical MD calculations to study the interactions, structure and dynamics of II-VI-type semiconductor nanoclusters solvated in a IL. For the setting and testing of the protocol, we take a semiconductor $(ZnS)_{12}$ nanocluster solvated by a $[EtSO_4][EMIM]$ IL as the referential system. We test the widely used PBE-GD3BJ exchange-correlation functional, several basis sets, and hydrogen bond acidities, and we choose the optimal combination based on geometrical and energetic criteria. All the DFT-based calculations, independently from the employed functional, basis set, and hydrogen acidity, show the formation of a strong coordination between an O atom of the anion of the IL and a Zn atom from the nanocluster. Then, we evaluate various classical force fields by classical optimization calculations and choose the optimal one. The strongest atomic inter-molecular interactions are reparametrized to fit the data obtained by DFT calculations. This set of new parameters properly describes the interaction energy scans of a $(ZnS)_{13}$ and $(ZnS)_{24}$ nanoclusters solvated by the $[EtSO_4][EMIM]$ IL, and thereby, supporting the transferability of the employed force field to study different size of nanoclusters (ZnS) solvated in the $[EtSO_4][EMIM]$ IL. The classical MD calculations show the formation of a structured solvation shell of nine $[EtSO_4^-]$ anions around the $(ZnS)_{12}$ nanocluster with no exchange of ions within this solvation shell for at least 5 ns.

Given that in the vast majority of known ILs the negative charge is more localized in the anion than the positive charge in the cation (as in the case of this study), similar type of interactions are expected in general within a system of a II-VI type of semiconductor nanocluster solvated in a IL. Therefore, this theoretical protocol is expected to be applicable to efficiently study such kind of solvated systems.

The observation of strong interactions between the Zn and O atoms is consistent with the APT charges, which shows different electric polarities for these atomic species. However, these results differ substantially with several previous experimental observations [51,55]. These observations together indicate that the nature of the interactions occurring between a nanoparticle and an IL are subtle and complex, and they may vary within the same nanoparticle family [54].

The overall picture shows that these nanoclusters get solvated by ILs with rather stable bonds (as confirmed by DFT calculations, classical MD simulations and bond analysis methods), with a first solvation shell conformed by nine IL pairs, covering a large part of the nanocluster surface. Therefore, the smallest model for the full solvation pattern of interest would be of roughly 300 atoms, out of the reach

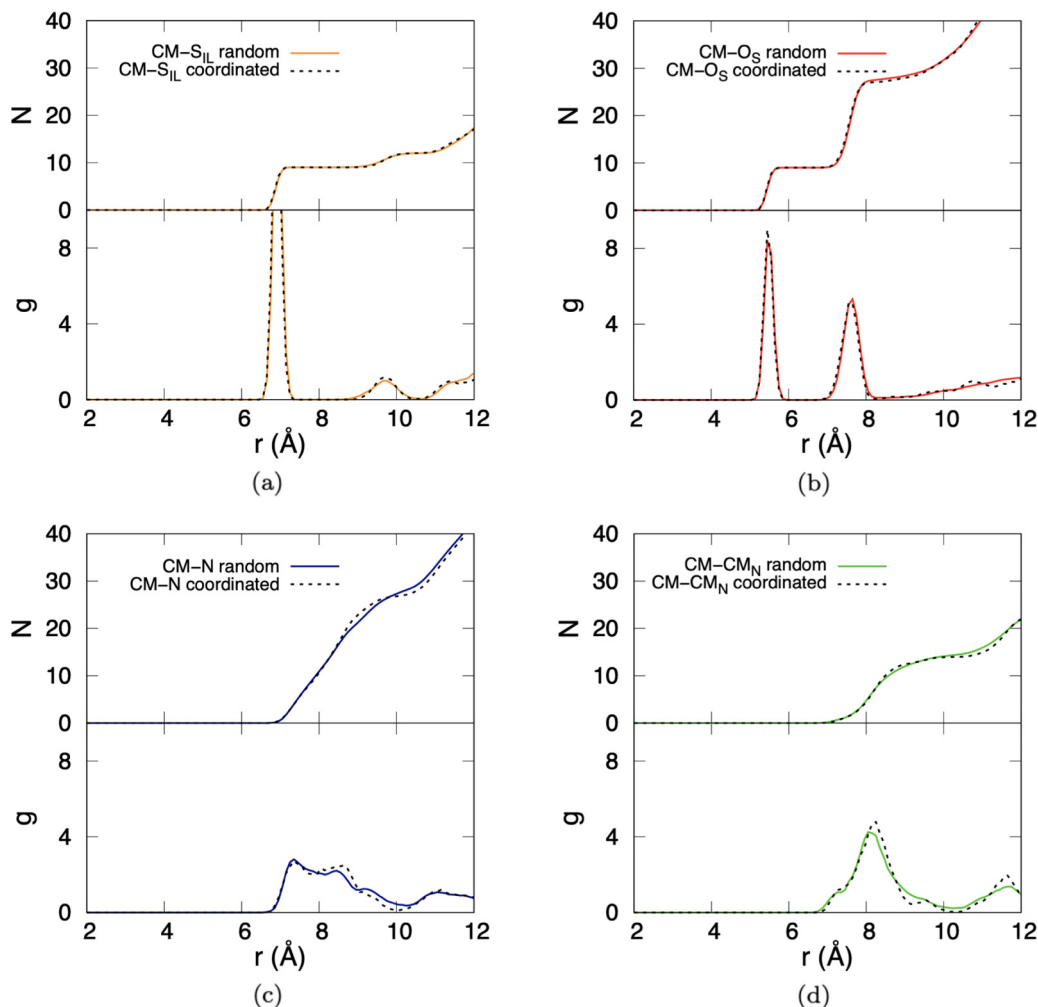


FIG. 9. Coordination number functions (upper panels) and radial distribution functions (lower panels) between the center of mass of the $(ZnS)_{12}$ nanocluster and several atomic species: (a) S_{IL} (orange) and (b) O_S (red) atoms from the $[EtSO_4^-]$ anion, and (c) N (blue) atom and (d) center of mass (green) of the $[EMIM^+]$ cations. Each function is calculated from the fully coordinated (dashed line) and random (continuous line) initial configurations.

of static DFT calculations as those performed in this paper. If particular interest on the quantum chemical nature of the nanocluster-IL bond was to be paid, then the fact that the first solvation shell seems to be rather well defined opens the possibility to efficiently study this kind of systems by means of *ab initio* molecular dynamics, considering only the first solvation shell explicitly, and including the bulk as an implicit solvation model. On the contrary, the inclusion of the bulk IL and therefore the long range interactions it establishes would require most likely classical molecular dynamics calculations, where the first solvation-shell interactions are no longer described at a quantum level, but rather parameterized. In this work, we have proposed the force-field parameters for such an approximation to the system, setting the grounds for expanding the system to larger nanoclusters solvated by more complex liquid systems.

ACKNOWLEDGMENTS

Financial support comes from Eusko Jaurlaritza through Project No. IT1254-19. The authors appreciate the techni-

cal and human support provided by SGIker (UPV/EHU, ERDF, EU). Dr. Daniel Arismendi, researcher of the Materials Physics Center in Donostia, is acknowledged for valuable discussions.

APPENDIX A: EXCHANGE-CORRELATION FUNCTIONAL, BASIS SET, AND IMPLICIT SOLVATION MODEL

Here we specify the different exchange-correlation functionals, basis sets, and hydrogen acidities employed in the DFT simulations:

(a) Four different *exchange-correlation functionals* were chosen among different functional types to ensure the results are consistent and stable. All of them account for dispersion interactions, due to the crucial role these interactions have in ILs [71,72,97]: (i) The semiempirical generalized gradient approximation (GGA)-based B97D pure functional including a dispersion term [98]. (ii) The GGA-based PBE exchange-correlation pure functional [99,100] combined with the D3 version of Grimme's dispersion term with the Becke-Johnson

damping [101] (PBE-GD3BJ). This particular functional has been found to yield good accuracy for IL systems in the literature [70–72]. (iii) The long-range corrected hybrid functional with dispersion correction wB97XD [102]. (iv) The meta-GGA-based M11 range-separated hybrid functional [103].

(b) We modify the number of the *basis set* for each subsystem, i.e., nanocluster and IL. We use a nomenclature describing the basis set employed for each subsystem with the form: nanocluster-basis set/IL-basis set. Unless specified, the electrons of the S atoms are described by the SKBJ(d) basis set previously developed in Ref. [21] based on the the SKBJ pseudopotentials [104,105]. Thereby, we refer to the part of the nomenclature related to the nanocluster by the basis set employed only for the electrons of the Zn atoms. Regarding the IL molecules, we modify the number of basis functions to describe the electrons from the C, N and O atoms, while the electrons of the H atoms are represented by a DZP. We employ the following basis sets: (i) the SKBJ(28)-P/SKBJ basis set, where the 28 core electrons of the Zn atom are represented by a SKBJ pseudopotential and the valence electrons by a DZP+d basis set as in Ref. [21]. The core electrons of the C, O and N atoms are described by a SKBJ pseudopotential and the valence electrons by a DZ basis set. (ii) The SKBJ(28)-P/SKBJ-P basis set, which only adds a polarization function to the valence electrons of the C, O and N of the previous SKBJ(28)-P/SKBJ basis set. (iii) The SKBJ(10)-P/DZP basis set, where the 10 inner electrons of the Zn atom are represented by a SKBJ pseudopotential, and the rest of the 20 electrons by a DZP+d basis function. The electrons of the C, O and N atoms are represented by a 6-31G(d,p) DZP basis set [106].

These basis sets have been chosen based on two criteria: first, the SKBJ(10)-P/DZP has already shown to reliably describe the $(\text{ZnS})_i$ nanoclusters in the gas phase [21] and the IL, both independently. In particular, Pople style double- ζ basis sets have been seen to give good results for ILs [70,71]. Second, the use of a large number of basis set functions would compromise the efficiency of DFT calculations where several IL molecules are included. Therefore, SKBJ(28)-P-based basis sets are included in the study in an attempt of defining a less demanding theory level, that would enable

these kind of calculations on larger nanoclusters in the future. Indeed, the possibility to carry out such kind of calculations is one of the objectives for which this theoretical protocol is designed.

In addition, QTAIM calculations are performed with (iv) the 6-31G(d,p) all-electron basis set, while some specific free-energy calculations are also done with (v) the 6-311++G(2df,2p) all-electron basis set (see main text).

(c) The *implicit solvation model* employed. The parameters of the SMD [74] method are taken from the generic IL solvation model, calculated from an average over 11 different ILs [107]: hydrogen bond acidity $\alpha = 0.229$, hydrogen bond basicity $\beta = 0.265$, static dielectric constant $\epsilon = 11.5$, index of refraction $n = 1.43$ and surface tension at the interface $\gamma = 61.24 \text{ cal mol}^{-1} \text{ \AA}^{-2}$. To observe possible differences in the results between the use of a general SMD parameter set and a characteristic parameter set to describe our particular IL, we employ two different values of the hydrogen bond acidity: $\alpha_g = 0.229$ and $\alpha_p = 0.440$. The former is obtained from the generic IL solvation model [107], while the latter was set to describe a [BMIM][CH₃SO₃] IL by the SMD method [108], similar to the IL studied in this work.

APPENDIX B: $(\text{ZnS})_{12}$ FORCE FIELD

The basic form of the interatomic potentials is similar in the three cases: the short-range non-Coulombic interaction between the i and j particles takes the Buckingham potential form:

$$U_{ij}^{\text{short}} = A \exp\left(\frac{-r_{ij}}{\rho}\right) - Cr_{ij}^{-6}. \quad (\text{B1})$$

A core-shell model is employed in the description of the S atom to account for possible polarization effects. These core and shell particles interact with each other by an harmonic potential:

$$U_{ij}^{\text{core-shell}} = \frac{1}{2}Kr_{ij}^2. \quad (\text{B2})$$

TABLE V. Implicit solvation (ΔG_S^1 and ΔG_S^2) free energies and implicit solvation free energy differences ($\Delta G_S^2 - \Delta G_S^1$) of a $(\text{ZnS})_{12}$ nanocluster and one pair of IL molecule obtained with three different basis sets and four exchange-correlation functionals.

Basis set	E_{xc}	ΔG_S^1 (kcal/mol)	ΔG_S^2 (kcal/mol)	$\Delta G_S^2 - \Delta G_S^1$ (kcal/mol)
SKBJ(28)-P/SKBJ	PBE-GD3BJ	-101.8	-99.4	2.4
	M11	-114.1	-115.7	-1.6
	B97D	-105.5	-105.9	-0.4
	wB97XD	-113.1	-115.5	-2.4
SKBJ(28)-P/SKBJ-P	PBE-GD3BJ	-99.7	-98.9	0.8
	M11	-114.3	-113.0	1.3
	B97D	-104.0	-104.0	0.0
	wB97XD	-112.1	-113.0	-0.9
SKBJ(10)-P/DZP	PBE-GD3BJ	-74.5	-73.2	1.3
	M11	-102.2	-104.2	-2.0
	B97D	-84.5	-84.1	0.4
	wB97XD	-88.4	-87.5	0.9

TABLE VI. Interaction (ΔG_1^{gas}) free energies of a (ZnS)₁₂ nanocluster and one pair of IL ions obtained with three different basis sets and four exchange-correlation functionals.

Basis set	E_{xc}	ΔG_1^{gas} (kcal/mol)
SKBJ(28)-P/SKBJ	PBE-GD3BJ	-28.2
	M11	-28.5
	B97D	-27.2
	wB97XD	-30.6
SKBJ(28)-P/SKBJ-P	PBE-GD3BJ	-26.7
	M11	-27.5
	B97D	-25.1
	wB97XD	-30.1
SKBJ(10)-P/DZP	PBE-GD3BJ	-25.5
	M11	-25.5
	B97D	-22.5
	wB97XD	-24.3

A three-body term is also included to account for directional-ity effects of the covalent bonds within the nanocluster:

$$U_{ijk} = \frac{1}{2}K_{\text{TB}}(\theta_{ijk} - \theta_0)^2, \quad (\text{B3})$$

where θ_{ijk} is the angle formed by the i , j and k particles. Each of the force fields are characterized by having different values of the charges of the particles and parameters A , ρ , C , K , and K_{TB} appearing in Eqs. (B1)–(B3). However, each one is also characterized by a main difference with respect to the others: Hamad *et al.* [81] add a new term Br_{ij}^{-9} to the short-range

potential in Eq. (B1) to describe a mixed Buckingham and Lenard-Jones 9-6 potential. Wright *et al.* [83] describe the Zn atom also by a core-shell model to account for possible polarization effects. Both, Namsani *et al.* [82] and Wright *et al.* [83] instead of using the harmonic three-body potential in Eq. (B3), they employ a harmonic potential with exponential decay:

$$U_{ijk} = \frac{1}{2}K_{\text{TB}}(\theta_{ijk} - \theta_0)^2 \exp\left(-\frac{r_{ij}}{\rho_1}\right) \exp\left(-\frac{r_{jk}}{\rho_2}\right). \quad (\text{B4})$$

APPENDIX C: FREE-ENERGY ANALYSIS

Table V shows the implicit solvation free energies obtained with different basis sets, exchange-correlation functionals and hydrogen acidities $\alpha_1 = 0.229$ and $\alpha_2 = 0.44$. The difference in solvation free energies obtained with the employed two hydrogen acidities are also shown.

Table VI shows the interaction free energies obtained with the different basis sets and exchange correlation functionals considered in this work.

APPENDIX D: GEOMETRICAL PARAMETERS BY DFT

Table VII shows the geometrical parameters obtained from the relaxed structure of the (ZnS)₁₂ nanocluster and one IL molecule in the gas phase [(ZnS)₁₂ + IL]_{gas} and implicitly solvated [(ZnS)₁₂ + IL]_{IL} with different basis sets and exchange-correlation functionals (E_{xc}). Here, we compare the geometrical parameters obtained with the SKBJ(10)-P/DZP basis set.

TABLE VII. Several geometrical parameters obtained from a relaxation calculation of a (ZnS)₁₂ nanocluster and one IL molecule in the gas phase [(ZnS)₁₂ + IL]_{gas} and implicitly solvated [(ZnS)₁₂ + IL]_{IL} with different basis sets and exchange-correlation functionals (E_{xc}).

System	Basis set	E_{xc}	$\langle d_1 \rangle$ (Å)	$\langle d_2 \rangle$ (Å)	$d_{\text{Zn-O}}$ (Å)	ϕ (°)	Θ (°)	$d_{\text{C-O}}$ (Å)
[(ZnS) ₁₂ + IL] _{gas}	SKBJ(28)-P/SKBJ	PBE-GD3BJ	2.348	2.268	1.935	134.655	-43.517	2.912
		M11	2.346	2.267	1.927	135.863	-34.271	2.988
		B97D	2.350	2.248	1.933	139.859	-32.199	3.020
		WB97XD	2.334	2.256	1.919	141.709	-33.927	3.001
	SKBJ(28)-P/SKBJ-P	PBE-GD3BJ	2.348	2.268	1.951	127.909	-50.610	2.894
		M11	2.345	2.267	1.952	127.068	-45.277	2.952
		B97D	2.350	2.248	1.944	131.028	-48.644	2.907
		WB97XD	2.333	2.256	1.931	131.072	-48.962	2.856
	SKBJ(10)-P/DZP	PBE-GD3BJ	2.337	2.247	2.013	128.059	-69.559	3.006
		M11	2.338	2.251	2.022	122.556	-47.317	2.943
		B97D	2.371	2.248	2.026	130.627	-65.534	2.991
		WB97XD	2.325	2.241	1.994	131.867	-68.061	2.991
[(ZnS) ₁₂ + IL] _{IL}	SKBJ(28)-P/SKBJ	PBE-GD3BJ	2.381	2.316	1.960	144.610	-54.878	3.110
		M11	2.383	2.309	1.946	146.492	-61.274	3.180
		B97D	2.309	2.296	1.964	142.775	-60.775	3.196
		WB97XD	2.370	2.302	1.953	145.550	-55.974	3.090
	SKBJ(28)-P/SKBJ-P	PBE-GD3BJ	2.380	2.316	1.990	133.607	-58.702	3.138
		M11	2.382	2.316	1.978	134.289	-58.906	2.968
		B97D	2.386	2.295	1.984	136.202	-58.402	3.056
		WB97XD	2.370	2.303	1.974	136.740	-58.743	3.044
	SKBJ(10)-P/DZP	PBE-GD3BJ	2.362	2.278	2.055	128.633	-63.968	3.115
		M11	2.373	2.298	2.047	133.135	-62.659	2.941
		B97D	2.400	2.288	2.081	130.703	-64.510	3.124
		WB97XD	2.353	2.272	2.042	132.868	-63.441	3.077

The geometrical distance parameters ($\langle d_1 \rangle$, $\langle d_2 \rangle$, d_{Zn-O} , and d_{C-O}) obtained with the B97D functional show the largest deviations with respect to the ones obtained with the rest of the functionals. If compared with the ones obtained with the PBE-GD3BJ functional, then the difference in d_{Zn-O} of the system in the gas phase and surrounded by the implicit IL is 0.013 Å and 0.026 Å, respectively. The largest differences in $\langle d_1 \rangle$ are: 0.034 Å in the gas phase, while 0.038 Å when surrounded by the implicit IL. d_{C-O} shows small differences when the system is in the gas phase and when the implicit solvent is included: 0.015 and 0.009 Å, respectively.

The results obtained with the M11 functional shows the following when compared to the ones obtained with the PBE-GD3BJ functional: $\langle d_1 \rangle$, $\langle d_2 \rangle$, and d_{Zn-O} distance parameters are similar, with differences smaller than 0.02 Å. The largest

distance deviation comes from the d_{C-O} distance parameter giving a 0.063 and 0.170 Å difference in the gas phase and implicitly solvated, respectively. The angular deviations are small for both parameters (ϕ and Θ): 5.503° and 12.242° in the gas phase, and 4.502° and 1.309° when implicitly solvated.

The comparison between the geometrical parameters obtained by the wB97XD and PBE-GD3BJ exchange-correlation functionals show large agreement: except for the case in which the system is implicitly solvated, where the difference in d_{C-O} is 0.038 Å, the rest of the geometrical distance parameter differences do not exceed 0.02 Å. The ϕ and Θ angles also show small differences: -3.808° and -1.498° in the gas phase respectively, while -4.235° and -0.526° when implicitly solvated, respectively.

-
- [1] A. Kampmann and D. Lincot, Photoelectrochemical study of thin film semiconductor heterostructures: Junction formation processes in CdS, *J. Electroanal. Chem.* **418**, 73 (1996).
- [2] Y. Loginov, K. Durose, H. Al-Allak, S. Galloway, S. Oktik, A. Brinkman, H. Richter, and D. Bonnet, Transmission electron microscopy of CdTe/CdS-based solar cells, *J. Cryst. Growth* **161**, 159 (1996).
- [3] A. Niemegeers and M. Burgelman, Effects of the Au/CdTe back contact on IV and CV characteristics of Au/CdTe/CdS/TcO solar cells, *J. Appl. Phys.* **81**, 2881 (1997).
- [4] K. Li, A. S. Wee, J. Lin, K. Tan, L. Zhou, S. Y. Li, Z. Feng, H. Chou, S. Kamra, and A. Rohatgi, A microstructural study on the surface and interface of CdTe/CdS solar cells, *J. Mater. Sci.: Mater. Electron.* **8**, 125 (1997).
- [5] K. Omura, A. Hanahusa, T. Arita, H. Higuchi, T. Aramoto, T. Nishio, S. Sibutani, S. Kumazawa, M. Murozono, Y. Yabuuchi *et al.*, Recent technical advances in thin-film CdS/CdTe solar cells, *Ren. Energy* **8**, 405 (1996).
- [6] C. Ferekides and J. Britt, CdTe solar cells with efficiencies over 15%, *Sol. Energy Mater. Sol. Cells* **35**, 255 (1994).
- [7] H. Chou, A. Rohatgi, N. Jokerst, E. Thomas, and S. Kamra, Copper migration in CdTe heterojunction solar cells, *J. Electron. Mater.* **25**, 1093 (1996).
- [8] S. Naseem, D. Nazir, R. Mumtaz, and K. Hussain, Evaporated thin films of CdS and CdTe: Optimization for photovoltaic applications, *J. Mater. Sci. Technology* **12**, 89 (1996).
- [9] R. Kisslinger, W. Hua, and K. Shankar, Bulk heterojunction solar cells based on blends of conjugated polymers with II–VI and IV–VI inorganic semiconductor quantum dots, *Polymers* **9**, 35 (2017).
- [10] J. Wilcoxon, T. Thurston, and J. Martin, Applications of metal and semiconductor nanoclusters as thermal and photocatalysts, *Nanostruct. Mater.* **12**, 993 (1999).
- [11] A. Hoffman, G. Mills, H. Yee, and M. Hoffmann, Q-sized cadmium sulfide: Synthesis, characterization, and efficiency of photoinitiation of polymerization of several vinylic monomers, *J. Phys. Chem.* **96**, 5546 (1992).
- [12] S. Kuwabata, K. Nishida, R. Tsuda, H. Inoue, and H. Yoneyama, Photochemical reduction of carbon dioxide to methanol using ZnS microcrystallite as a photocatalyst in the presence of methanol dehydrogenase, *J. Electrochem. Soc.* **141**, 1498 (1994).
- [13] J. Jie, W. Zhang, I. Bello, C.-S. Lee, and S.-T. Lee, One-dimensional II–VI nanostructures: Synthesis, properties and optoelectronic applications, *Nano today* **5**, 313 (2010).
- [14] D. Nesheva and H. Hofmeister, Formation of CdSe nanoclusters in SiOx thin films, *Solid State Commun.* **114**, 511 (2000).
- [15] S. Kumar and T. Nann, Shape control of II–VI semiconductor nanomaterials, *Small* **2**, 316 (2006).
- [16] C. Feldmann, Metastable solids-terra incognita awaiting discovery, *Angew. Chem. Int. Ed.* **52**, 7610 (2013).
- [17] H.-Y. Lu, S.-Y. Chu, and S.-S. Tan, The characteristics of low-temperature-synthesized ZnS and ZnO nanoparticles, *J. Cryst. Growth* **269**, 385 (2004).
- [18] S. Biswas and S. Kar, Fabrication of ZnS nanoparticles and nanorods with cubic and hexagonal crystal structures: A simple solvothermal approach, *Nanotechnology* **19**, 045710 (2008).
- [19] F. Huo, Y. Wang, C. You, W. Deng, F. Yang, and Y. Pu, Phase- and size-controllable synthesis with efficient photocatalytic activity of ZnS nanoparticles, *J. Mater. Sci.* **52**, 5626 (2017).
- [20] S. Hamad, C. R. A. Catlow, E. Spano, J. M. Matxain, and J. M. Ugalde, Structure and properties of ZnS nanoclusters, *J. Phys. Chem. B* **109**, 2703 (2005).
- [21] J. M. Matxain, J. E. Fowler, and J. M. Ugalde, Small clusters of II–VI materials: Zn_iS_i , $i = 1 - 9$, *Phys. Rev. A* **61**, 053201 (2000).
- [22] J. M. Matxain, L. A. Eriksson, J. M. Mercero, J. M. Ugalde, E. Spano, S. Hamad, and C. R. A. Catlow, Electronic excitation energies of znisi nanoparticles, *Nanotechnology* **17**, 4100 (2006).
- [23] J. M. Matxain, L. A. Eriksson, E. Formoso, M. Piris, and J. M. Ugalde, Endohedral ($x@zn_izisi$) $i = 4-160$, \pm nanoclusters, $x = li, na, k, cl, br$, *J. Phys. Chem. C* **111**, 3560 (2007).
- [24] J. M. Matxain, E. Formoso, J. M. Mercero, M. Piris, X. Lopez, and J. M. Ugalde, Magnetic endohedral transition-metal-doped semiconducting-nanoclusters, *Chem. A: Eur. J.* **14**, 8547 (2008).
- [25] E. Jimenez-Izal, J. M. Matxain, M. Piris, and J. M. Ugalde, Structure and stability of the endohedrally doped ($x@cd_izisi$) $i = 4, 9, 12, 15, 16$ $q = 0, \pm 1$, $x = na, k, cl, br$, nanoclusters, *J. Phys. Chem. C* **114**, 2476 (2010).

- [26] E. Jimenez-Izal, J. M. Azpiroz, R. Gupta, J. M. Matxain, and J. M. Ugalde, CdS nanoclusters doped with divalent atoms, *J. Molec. Model.* **20**, 2227 (2014).
- [27] E. Jimenez-Izal, J. M. Matxain, M. Piris, and J. M. Ugalde, Self-assembling endohedrally doped CdS nanoclusters: new porous solid phases of CdS, *Phys. Chem. Chem. Phys.* **14**, 9676 (2012).
- [28] R. Xie, Z. Li, and X. Peng, Nucleation kinetics vs chemical kinetics in the initial formation of semiconductor nanocrystals, *J. Am. Chem. Soc.* **131**, 15457 (2009).
- [29] P. Han and G. Bester, First-principles calculation of the electron-phonon interaction in semiconductor nanoclusters, *Phys. Rev. B* **85**, 235422 (2012).
- [30] M. Del Ben, R. W. Havenith, R. Broer, and M. Stener, Density functional study on the morphology and photoabsorption of CdSe nanoclusters, *J. Phys. Chem. C* **115**, 16782 (2011).
- [31] W.-Z. Xiao, L.-I. Wang, Q.-Y. Rong, G. Xiao, and B. Meng, Magnetism in undoped ZnS studied from density functional theory, *J. Appl. Phys.* **115**, 213905 (2014).
- [32] D. Gao, G. Yang, J. Zhang, Z. Zhu, M. Si, and D. Xue, d₀ ferromagnetism in undoped sphalerite ZnS nanoparticles, *Appl. Phys. Lett.* **99**, 052502 (2011).
- [33] S. Pal, B. Goswami, and P. Sarkar, Size-dependent properties of hollow ZnS nanoclusters, *J. Phys. Chem. C* **112**, 6307 (2008).
- [34] M. Jothibas, C. Manoharan, S. J. Jeyakumar, P. Praveen, I. K. Punithavathy, and J. P. Richard, Synthesis and enhanced photocatalytic property of ni doped ZnS nanoparticles, *Solar Energy* **159**, 434 (2018).
- [35] J. Luczak, M. Paszkiewicz, A. Krukowska, A. Malankowska, and A. Zaleska-Medynska, Ionic liquids for nano- and microstructures preparation. Part 2: Application in synthesis, *Adv. Colloid Interface Sci.* **227**, 1 (2016).
- [36] J. Luczak, M. Paszkiewicz, A. Krukowska, A. Malankowska, and A. Zaleska-Medynska, Ionic liquids for nano- and microstructures preparation. part 1: Properties and multifunctional role, *Adv. Colloid Interface Sci.* **230**, 13 (2016).
- [37] Z. Li, Z. Jia, Y. Luan, and T. Mu, Ionic liquids for synthesis of inorganic nanomaterials, *Curr. Opin. Solid State Mater. Sci.* **12**, 1 (2008).
- [38] H. Sajjadi, A. Modaressi, P. Magri, U. Domańska, M. Sindt, J.-L. Mieloszynski, F. Mutelet, and M. Rogalski, Aggregation of nanoparticles in aqueous solutions of ionic liquids, *J. Mol. Liq.* **186**, 1 (2013).
- [39] J. Dupont and J. D. Scholten, On the structural and surface properties of transition-metal nanoparticles in ionic liquids, *Chem. Soc. Rev.* **39**, 1780 (2010).
- [40] G. Machado, J. D. Scholten, T. d. Vargas, S. R. Teixeira, L. Ronchi, and J. Dupont, Structural aspects of transition-metal nanoparticles in imidazolium ionic liquids, *Int. J. Nanotechn.* **4**, 541 (2007).
- [41] A. Safavi and S. Zeinali, Synthesis of highly stable gold nanoparticles using conventional and geminal ionic liquids, *Colloids Surf., A* **362**, 121 (2010).
- [42] M. Behboudnia, A. Habibi-Yangjeh, Y. Jafari-Tarzanag, and A. Khodayari, Preparation and characterization of monodispersed nanocrystalline ZnS in water-rich [emim] etso₄ ionic liquid using ultrasonic irradiation, *J. Cryst. Growth* **310**, 4544 (2008).
- [43] M. Barjasteh-Moghaddam and A. Habibi-Yangjeh, Effect of operational parameters on photodegradation of methylene blue on ZnS nanoparticles prepared in presence of an ionic liquid as a highly efficient photocatalyst, *J. Iranian Chem. Soc.* **8**, S169 (2011).
- [44] Y. Wu, X. Hao, J. Yang, F. Tian, and M. Jiang, Ultrasound-assisted synthesis of nanocrystalline ZnS in the ionic liquid [bmim] bf₄, *Mater. Lett.* **60**, 2764 (2006).
- [45] J. X. Yang, S. M. Wang, X. L. Zhao, Y. P. Tian, S. Y. Zhang, B. K. Jin, X. P. Hao, X. Y. Xu, X. T. Tao, and M. H. Jiang, Preparation and characterization of ZnS nanocrystal from zn (ii) coordination polymer and ionic liquid, *J. Cryst. Growth* **310**, 4358 (2008).
- [46] Z. Tshemese, S. Mlowe, N. Revaprasadu, and N. Deenadayalu, Synthesis of CdS quantum dots in an imidazolium based ionic liquid, *Mater. Sci. Semiconductor Process.* **71**, 258 (2017).
- [47] K. Yao, W. Lu, and J. Wang, Ionic liquid-assisted synthesis, structural characterization, and photocatalytic performance of CdS nanocrystals, *Mater. Chem. Phys.* **130**, 1175 (2011).
- [48] G. Zhang, W. Luo, Q. Qin, Y. Liu, C. Jin, J. Hao, J. Zhang, and W. Zheng, Ionic liquid bifunctionally modulated aggregation-coalescence mechanism to synthesize SnSe single-crystal nanorod/nanoparticle core shell nanostructures and single-crystal nanorods for optoelectronics, *Cryst. Eng. Commun.* **20**, 1141 (2018).
- [49] L. Das, A. Guleria, S. Neogy, and S. Adhikari, Porous nanostructures of SnSe: role of ionic liquid, tuning of nanomorphology and mechanistic studies, *RSC Adv.* **6**, 92934 (2016).
- [50] A. Guleria, A. K. Singh, M. C. Rath, S. Adhikari, and S. K. Sarkar, Islands of CdSe nanoparticles within Se nanofibers: A room temperature ionic liquid templated synthesis, *Dalton Trans.* **42**, 15159 (2013).
- [51] A. Guleria, A. K. Singh, M. C. Rath, S. K. Sarkar, and S. Adhikari, The role of structural and fluidic aspects of room temperature ionic liquids in influencing the morphology of CdSe nano/microstructures grown in situ, *Dalton Trans.* **43**, 11843 (2014).
- [52] M. Green, P. Rahman, and D. Smyth-Boyle, Ionic liquid passivated CdSe nanocrystals, *Chem. Commun.* **43**, 574 (2007).
- [53] K. Biswas and C. N. R. Rao, Use of ionic liquids in the synthesis of nanocrystals and nanorods of semiconducting metal chalcogenides, *Chem. A: Eur. J.* **13**, 6123 (2007).
- [54] N. Dengo, A. Vittadini, M. M. Natile, and S. Gross, In-depth study of ZnS nanoparticle surface properties with a combined experimental and theoretical approach, *J. Phys. Chem. C* **124**, 7777 (2020).
- [55] M. Barzegar, A. Habibi-Yangjeh, and M. Behboudnia, Ultrasonic-assisted preparation and characterization of CdS nanoparticles in the presence of a halide-free and low-cost ionic liquid and photocatalytic activity, *J. Phys. Chem. Solids* **71**, 1393 (2010).
- [56] M. Zhang, L.-J. Yu, Y.-F. Huang, J.-W. Yan, G.-K. Liu, D.-Y. Wu, Z.-Q. Tian, and B.-W. Mao, Extending the shell-isolated nanoparticle-enhanced raman spectroscopy approach to interfacial ionic liquids at single crystal electrode surfaces, *Chem. Commun.* **50**, 14740 (2014).
- [57] P. Cheng, C. Liu, Y. Yang, and S. Huang, First-principle investigation of the interactions between Pt_xRu_{55-x} (x =

- 0, 13, 42, 55) nanoparticles and [BMIM][PF₆] ionic liquid, *Chem. Phys.* **452**, 1 (2015).
- [58] J.-M. Andanson and A. Baiker, Interactions of 1-ethyl-3-methylimidazolium trifluoromethanesulfonate ionic liquid with alumina nanoparticles and organic solvents studied by infrared spectroscopy, *J. Phys. Chem. C* **117**, 12210 (2013).
- [59] D. S. Frost and L. L. Dai, Molecular dynamics simulations of nanoparticle self-assembly at ionic liquid–water and ionic liquid–oil interfaces, *Langmuir* **27**, 11339 (2011).
- [60] D. L. Cheung, Molecular dynamics study of nanoparticle stability at liquid interfaces: Effect of nanoparticle–solvent interaction and capillary waves, *J. Chem. Phys.* **135**, 054704 (2011).
- [61] A. S. Pensado and A. A. Pádua, Solvation and stabilization of metallic nanoparticles in ionic liquids, *Angew. Chem. Int. Ed.* **50**, 8683 (2011).
- [62] Z. He and P. Alexandridis, Nanoparticles in ionic liquids: Interactions and organization, *Phys. Chem. Chem. Phys.* **17**, 18238 (2015).
- [63] D. S. Frost and L. L. Dai, Molecular dynamics simulations of charged nanoparticle self-assembly at ionic liquid–water and ionic liquid–oil interfaces, *J. Chem. Phys.* **136**, 084706 (2012).
- [64] D. S. Frost, M. Machas, and L. L. Dai, Molecular dynamics studies on the adaptability of an ionic liquid in the extraction of solid nanoparticles, *Langmuir* **28**, 13924 (2012).
- [65] V. Velachi, D. Bhandary, J. K. Singh, and M. N. D. Cordeiro, Striped gold nanoparticles: New insights from molecular dynamics simulations, *J. Chem. Phys.* **144**, 244710 (2016).
- [66] G. Salas, A. Podgoršek, P. S. Campbell, C. C. Santini, A. A. Pádua, M. F. C. Gomes, K. Philippot, B. Chaudret, and M. Turmine, Ruthenium nanoparticles in ionic liquids: Structural and stability effects of polar solutes, *Phys. Chem. Chem. Phys.* **13**, 13527 (2011).
- [67] S. Sarangi, B. Bhargava, and S. Balasubramanian, Nanoclusters of room temperature ionic liquids: A molecular dynamics simulation study, *Phys. Chem. Chem. Phys.* **11**, 8745 (2009).
- [68] M. Abbaspour, H. Akbarzadeh, P. Yousefi, and M. Razmkhah, Investigation of solvation of iron nanoclusters in ionic liquid 1-butyl-1, 1, 1-trimethylammonium methane sulfonate using molecular dynamics simulations: Effect of cluster size at different temperatures, *J. Colloid Interface Sci.* **504**, 171 (2017).
- [69] M. J. Frisch, G. W. Trucks, H. B. Schlegel, G. E. Scuseria, M. A. Robb, J. R. Cheeseman, G. Scalmani, V. Barone, G. A. Petersson, H. Nakatsuji, X. Li, M. Caricato, A. V. Marenich, J. Bloino, B. G. Janesko, R. Gomperts, B. Mennucci, H. P. Hratchian, J. V. Ortiz, A. F. Izmaylov *et al.*, *Gaussian 16 Revision C.01* (Gaussian Inc., Wallingford, CT, 2016).
- [70] S. Zahn, D. R. MacFarlane, and E. I. Izgorodina, Assessment of Kohn–Sham density functional theory and Møller–Plesset perturbation theory for ionic liquids, *Phys. Chem. Chem. Phys.* **15**, 13664 (2013).
- [71] E. I. Izgorodina, U. L. Bernard, and D. R. MacFarlane, Ion-pair binding energies of ionic liquids: can dft compete with *ab initio*-based methods? *J. Phys. Chem. A* **113**, 7064 (2009).
- [72] K. Karu, M. Mišin, H. Ers, J. Sun, and V. Ivaništšev, Performance of scan density functional for a set of ionic liquid ion pairs, *Int. J. Quantum Chem.* **118**, e25582 (2018).
- [73] E. Balantseva, G. Berlier, B. Camino, M. Lessio, and A. M. Ferrari, Surface properties of ZnS nanoparticles: A combined DFT and experimental study, *J. Phys. Chem. C* **118**, 23853 (2014).
- [74] A. V. Marenich, C. J. Cramer, and D. G. Truhlar, Universal solvation model based on solute electron density and on a continuum model of the solvent defined by the bulk dielectric constant and atomic surface tensions, *J. Phys. Chem. B* **113**, 6378 (2009).
- [75] A. E. Reed, L. A. Curtiss, and F. Weinhold, Intermolecular interactions from a natural bond orbital, donor-acceptor viewpoint, *Chem. Rev.* **88**, 899 (1988).
- [76] F. Weinhold, C. Landis, and C. U. Press, *Valency and Bonding: A Natural Bond Orbital Donor-Acceptor Perspective* (Cambridge University Press, Cambridge, UK, 2005).
- [77] R. Bader and R. Bader, *Atoms in Molecules: A Quantum Theory*, International series of monographs on chemistry (Clarendon Press, Oxford, UK, 1990).
- [78] C. Matta and R. Boyd, Quantum theory of atoms in molecules: recent progress in theory and application, *An Introduction to the Quantum Theory of Atoms in Molecules* (Clarendon Press, Oxford, UK, 2007).
- [79] T. A. Keith, Aimall (version 13.05.06) (TK Gristmill Software, Overland Park, KS, 2013).
- [80] S. Plimpton, *Fast parallel algorithms for short-range molecular dynamics*, Tech. Rep. (Sandia National Labs, Albuquerque, NM, 1993).
- [81] S. Hamad, S. Cristol, and C. R. A. Catlow, Surface structures and crystal morphology of ZnS: Computational study, *J. Phys. Chem. B* **106**, 11002 (2002).
- [82] S. Namsani, N. N. Nair, and J. K. Singh, Interaction potential models for bulk ZnS, ZnS nanoparticle, and ZnS nanoparticle-pmma from first-principles, *J. Comput. Chem.* **36**, 1176 (2015).
- [83] K. Wright and J. D. Gale, Interatomic potentials for the simulation of the zinc-blende and wurtzite forms of ZnS and CdS: Bulk structure, properties, and phase stability, *Phys. Rev. B* **70**, 035211 (2004).
- [84] J. D. Gale, Gulp: A computer program for the symmetry-adapted simulation of solids, *J. Chem. Soc. Faraday Trans.* **93**, 629 (1997).
- [85] J. D. Gale and A. L. Rohl, The general utility lattice program (gulp), *Mol. Simul.* **29**, 291 (2003).
- [86] J.-P. Ryckaert, G. Ciccotti, and H. J. Berendsen, Numerical integration of the cartesian equations of motion of a system with constraints: Molecular dynamics of n-alkanes, *J. Comput. Phys.* **23**, 327 (1977).
- [87] R. W. Hockney and J. W. Eastwood, *Computer Simulation Using Particles* (CRC Press, New York, 1988).
- [88] A. A. Pádua, M. F. Costa Gomes, and J. N. Canongia Lopes, Molecular solutes in ionic liquids: A structural perspective, *Acc. Chem. Res.* **40**, 1087 (2007).
- [89] C. Cervinka, A. A. Pádua, and M. Fulem, Thermodynamic properties of selected homologous series of ionic liquids calculated using molecular dynamics, *J. Phys. Chem. B* **120**, 2362 (2016).
- [90] K. Goloviznina, J. N. Canongia Lopes, M. Costa Gomes, and A. A. Pádua, Transferable, polarizable force field for ionic liquids, *J. Chem. Theory Comput.* **15**, 5858 (2019).
- [91] P. Mitchell and D. Fincham, Shell model simulations by adiabatic dynamics, *J. Phys.: Condens. Matter* **5**, 1031 (1993).

- [92] G. Lamoureux and B. Roux, Modeling induced polarization with classical drude oscillators: Theory and molecular dynamics simulation algorithm, *J. Chem. Phys.* **119**, 3025 (2003).
- [93] M. Lísal, Z. Chval, J. Storch, and P. Izák, Towards molecular dynamics simulations of chiral room-temperature ionic liquids, *J. Mol. Liq.* **189**, 85 (2014).
- [94] E. Rezabal and T. Schäfer, Ionic liquids as solvents of polar and non-polar solutes: Affinity and coordination, *Phys. Chem. Chem. Phys.* **17**, 14588 (2015).
- [95] S. J. Grabowski, Relationships between QTAIM and the decomposition of the interaction energy—comparison of different kinds of hydrogen bond, in *Quantum Theory of Atoms in Molecules: From Solid State to DNA and Drug Design* (Wiley, New York, NY, 2007), p. 453.
- [96] A. Becke, *The Quantum Theory of Atoms in Molecules: From Solid State to DNA and Drug Design* (Wiley, New York, NY, 2007).
- [97] E. Rezabal and T. Schäfer, First principle approach to solvation by methylimidazolium-based ionic liquids, *J. Phys. Chem. B* **117**, 553 (2013).
- [98] S. Grimme, Semiempirical GGA-type density functional constructed with a long-range dispersion correction, *J. Comput. Chem.* **27**, 1787 (2006).
- [99] J. P. Perdew, K. Burke, and M. Ernzerhof, Generalized Gradient Approximation Made Simple, *Phys. Rev. Lett.* **77**, 3865 (1996).
- [100] J. Perdew, K. Burke, and M. Ernzerhof, Generalized Gradient Approximation Made Simple [Phys. Rev. Lett. **77**, 3865 (1996)], *Phys. Rev. Lett.* **78**, 1396 (1997).
- [101] S. Grimme, S. Ehrlich, and L. Goerigk, Effect of the damping function in dispersion corrected density functional theory, *J. Comput. Chem.* **32**, 1456 (2011).
- [102] J.-D. Chai and M. Head-Gordon, Long-range corrected hybrid density functionals with damped atom–atom dispersion corrections, *Phys. Chem. Chem. Phys.* **10**, 6615 (2008).
- [103] R. Peverati and D. G. Truhlar, Improving the accuracy of hybrid meta-GGA density functionals by range separation, *J. Phys. Chem. Lett.* **2**, 2810 (2011).
- [104] W. J. Stevens, M. Krauss, H. Basch, and P. G. Jasien, Relativistic compact effective potentials and efficient, shared-exponent basis sets for the third-, fourth-, and fifth-row atoms, *Can. J. Chem.* **70**, 612 (1992).
- [105] W. J. Stevens, H. Basch, and M. Krauss, Compact effective potentials and efficient shared-exponent basis sets for the first- and second-row atoms, *J. Chem. Phys.* **81**, 6026 (1984).
- [106] W. J. Hehre, R. Ditchfield, and J. A. Pople, Self-consistent molecular orbital methods. XII. Further extensions of Gaussian-type basis sets for use in molecular orbital studies of organic molecules, *J. Chem. Phys.* **56**, 2257 (1972).
- [107] V. S. Bernales, A. V. Marenich, R. Contreras, C. J. Cramer, and D. G. Truhlar, Quantum mechanical continuum solvation models for ionic liquids, *J. Phys. Chem. B* **116**, 9122 (2012).
- [108] R. Contreras, A. Aizman, R. A. Tapia, and A. Cerda-Monje, Lewis molecular acidity of ionic liquids from empirical energy–density models, *J. Phys. Chem. B* **117**, 1911 (2013).